

Global Characteristics of Stream Flow Seasonality and Variability

MICHAEL D. DETTINGER

U.S. Geological Survey, Scripps Institution of Oceanography, La Jolla, California

HENRY F. DIAZ

NOAA/OAR/Climate Diagnostics Center, Boulder, Colorado

(Manuscript received 20 May 1999, in final form 8 March 2000)

ABSTRACT

Monthly stream flow series from 1345 sites around the world are used to characterize geographic differences in the seasonality and year-to-year variability of stream flow. Stream flow seasonality varies regionally, depending on the timing of maximum precipitation, evapotranspiration, and contributions from snow and ice. Lags between peaks of precipitation and stream flow vary smoothly from long delays in high-latitude and mountainous regions to short delays in the warmest sectors. Stream flow is most variable from year to year in dry regions of the southwest United States and Mexico, the Sahel, and southern continents, and it varies more (relatively) than precipitation in the same regions. Tropical rivers have the steadiest flows. El Niño variations are correlated with stream flow in many parts of the Americas, Europe, and Australia. Many stream flow series from North America, Europe, and the Tropics reflect North Pacific climate, whereas series from the eastern United States, Europe, and tropical South America and Africa reflect North Atlantic climate variations.

1. Introduction

In their global compendium of mean annual precipitation, evaporation, and runoff rates, Baumgartner and Reichel (1975) commented that “for mankind and terrestrial life, freshwater supplies and exchanges in the hydrological cycle are plainly of special interest.” Motivating their work, and ours, is the recognition that hydrologic fluxes from and across the earth’s land surfaces do not vary in isolation from basin to basin nor even from region to region but rather are parts of a broad tapestry of interwoven moisture fluxes that spans the globe. As more and more studies have made progress toward integration and prediction of stream flow conditions on regional and larger scales (e.g., Probst and Tardy 1987, 1989; Depetris and Kempe 1990; Redmond and Koch 1991; Cayan and Webb 1992; Chiew et al. 1994; Eltahir 1996; Guetter and Georgakakos 1996; Hagemann and Dumenil 1996; McKerchar et al. 1996), often by relating stream flow to global climatic processes and precursors, the need for a large-scale depiction of the patterns of seasonality and interannual variability of stream flow from all of the earth’s land sur-

faces has become more pressing. Both the seasonality and year-to-year variations of global stream flows must be catalogued to understand linkages between basins and regions, and across time.

Although other groups have provided analyses of mean flows (e.g., Baumgartner and Reichel 1975; van der Leeden 1975; Legates and Mather 1992; Perry et al. 1996), the current study uses stream flow data to illustrate some of the basic patterns of stream flow seasonality, runoff generation, and climatic connections. Also in contrast to the current study, McMahon et al. (1992) analyzed annual stream flow variations in continental-scale comparisons, and Kalinin (1971) focused on annual Northern Hemisphere stream flows, whereas this paper considers variations within the continental areas and at timescales both shorter than and longer than annual. In a sense, this paper picks up where Baumgartner and Reichel (1975) left off, with respect to stream flow, by describing variations, rather than mean annual totals, of streamflow on a global scale. This preliminary description of stream flow variability is intended to provide a sketch of the large-scale context for the many, more detailed regional hydrologic investigations in the literature today. Because of the relatively large number of rivers represented in the dataset, spatial characteristics of stream flow variability are represented in somewhat more detail, but with less extrapolation, than the groundbreaking analyses of global stream flow distributions by Korzun (1978).

Corresponding author address: Michael D. Dettinger, U.S. Geological Survey, Scripps Institution of Oceanography, Dept. 0224, University of California, San Diego, 9500 Gilman Drive, La Jolla, CA 92093-0224.
E-mail: mddettin@usgs.gov

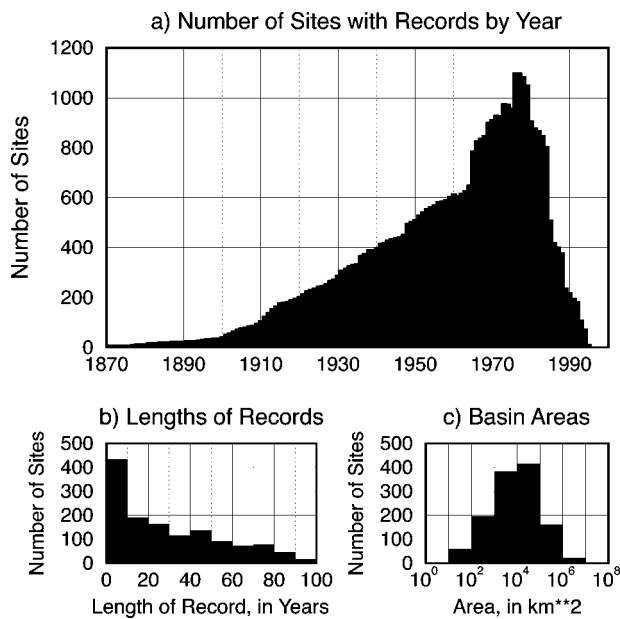


FIG. 1. Numbers of gauging sites with (a) stream flow records each year, (b) various lengths of record, and (c) various basin areas.

2. Global stream flow and precipitation data

The seasonality and variability of stream flow timing, stream flow amounts, and ratios of runoff to precipitation are analyzed here using a newly compiled, global dataset of monthly stream flow series. The global stream flow set currently contains series from 1345 gauging stations but is being augmented as additional series are obtained and digitized. The number of stations with stream flow records for each year beginning in 1870 is shown in Fig. 1a; lengths of records are summarized in Fig. 1b. These records come from a variety of sources listed in the acknowledgments and, unless otherwise noted, are from freely distributable (public domain) sources. The series have been merged in a common format, duplicate series have been identified and removed, and series that include unrealistic trends or obviously unnatural values and changes have been either removed or edited to remove unrealistic or the most clearly human-influenced segments. The editing of the time series, however, was restrained in this regard, because future analyses may find useful information even in the observations from heavily managed streams. Thus, this dataset is not limited strictly to rivers that have no human influences, but it has had the most blatantly changed river regimes and bad data points removed (details are available from the authors upon request). The dataset is not necessarily comprehensive in any given region [e.g., only a subset of the U.S. Hydroclimatic Data Network (Slack and Landwehr 1992) is included] and only includes up-to-date observations where those observations were readily available.

The spatial distributions of stream flow records of various lengths are shown in Fig. 2. At least some record

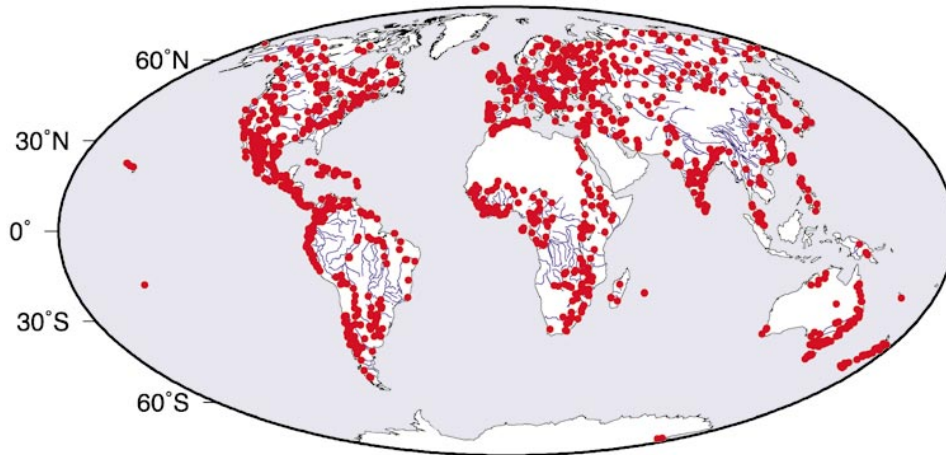
(Fig. 2a) is present on all continents and several of the larger islands. Notable gaps in the coverage of the present dataset include a large part of the Amazon basin [for which we have use of some proprietary records, courtesy of Dr. J. Marengo and Eletronorte (Centrais Elétricas do Norte do Brasil, S.A.) and Eletrobrás (Centrais Elétricas Brasileiras, S.A.)]; the Sahara, Arabian, South African, and Australian drylands; and interior China and central Asia. Twenty or more years of stream flow data (Figs. 1b and 2b) are available at 734 sites from many regions including Australia, the Sahel, India, and, especially, North America, Europe, and Russia. Even longer records (e.g., Fig. 2c) are available primarily from rivers in North America, Europe, eastern Australia, and the Nile system; 228 sites have 720 months or more of stream flow record. The average length of record is 318 months. A more extensive data collection (in some areas) is available from the World Meteorological Organization's Global Runoff Data Center, but distribution of those data has been substantially restricted and did not fit our desire for a compilation that could be traded informally with colleagues.

Basin areas are known for 92% of the sites. Together those sites constitute an area equivalent to 30% of the earth's land surface, although basins overlap so that the nonoverlapping coverage is closer to 22%. Basin areas range from 2 to 4 600 000 km², with 65% of the basins between 10³ and 10⁵ km² (Fig. 1c). For sites with known basin areas, monthly runoff rates defined as the monthly stream flow divided by the basin area were computed and used as an intensive measure (to complement the extensive measure, stream flow) in some of the following analyses. The global distribution of runoff rates is assessed in section 4.

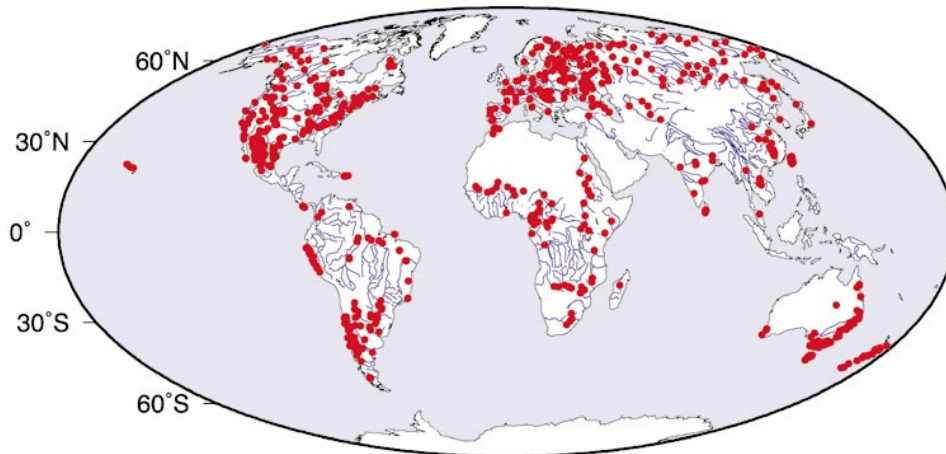
As part of quality-control checks on the dataset, Kendall's tau nonparametric tests (Press et al. 1989) were made for trends in the stream flow series at each site that has more than 40 yr of record. In general, the number of sites at which statistically significant trends could be identified (null hypothesis of no trend could be rejected at 99% confidence levels) in the 391 sites analyzed was small (14% of the series); significant positive trends were found at 6% of the sites and negative trends at 7%. Where trends were indicated (not shown here), they tended to form spatial clusters that include several different river basins in close proximity, especially when seasonal rather than annual totals were tested for trends. Indications of trends were found in central Canada and the Rocky Mountains, on the Nile and the Sahel, in Paraguay, and in western Russia. Detailed local analyses will be required to determine better the significance and causes of these trends [see, e.g., Marengo et al. (1998) for an example of the difficulties in separating out the causes of such trends]. Overall, however, the dataset probably is not unduly influenced by human activities or observational changes in the form of extraneous trends.

To characterize the moisture inputs that drive global

a) SITES WITH ANY STREAMFLOW DATA



b) SITES WITH MORE THAN 240 MONTHS OF STREAMFLOW DATA



c) SITES WITH MORE THAN 720 MONTHS OF STREAMFLOW DATA

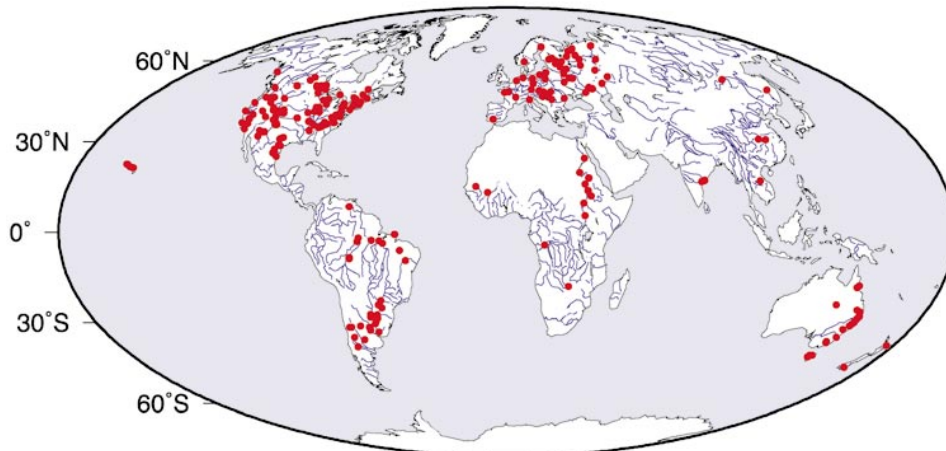


FIG. 2. Locations of gauging sites in the global stream flow set used here with (a) any stream flow data, (b) more than 20 yr of data, and (c) more than 60 yr of data.

stream flow variations and, in a sense, to verify those variations, global monthly precipitation mean and anomaly series for land areas from 1880 to 1992 (Eischeid et al. 1995) on a $5^\circ \times 5^\circ$ grid were compared with the stream flow series. The global precipitation means and anomalies were interpolated onto the $5^\circ \times 5^\circ$ grid from mean monthly precipitation totals and deviations from period-of-record mean monthly precipitation totals, respectively, at 5328 stations. The station records were tested individually and inspected visually for discontinuities and other nonclimatic biases by Eischeid et al. (1995). Preparation and quality control are described in the original reference (Eischeid et al. 1991); however, the data are subject to possible measurement biases, such as gauge undercatch because of wind effects, as are nearly all meteorological (and hydrological) measurements. The precipitation data are used here to estimate precipitation seasonality for comparison with stream flow timing and to estimate differences in annual and longer precipitation rates that affect long-term runoff variations. On these timescales, precipitation measurement biases are believed to be present but more or less stationary. Most of the weather stations are located at lower altitudes, however, so that the precipitation values have a low-altitude bias relative to many of the river basins represented in the global stream flow set, which, in contrast, commonly are fed by relatively high altitude catchments. This contrast in the altitudes represented by the two sets of observations results in some apparent discrepancies (to be discussed later) between estimates of runoff generated per unit basin area and the available precipitation observations in basins with large orographic-precipitation gradients.

Seasonal variations in evaporation can play nearly as great a role in determining stream flow seasonality as does precipitation in many areas. To account for this influence, stream flow timing also will be compared with the seasonality of precipitation-minus-evaporation estimates from the recently released reanalyzed global-climate precipitation and surface latent heat fluxes from 1948–98 on a T62 grid of approximately $2.5^\circ \text{ lat} \times 2.5^\circ \text{ long}$ (Kalnay et al. 1996), from the National Centers for Environmental Prediction (NCEP) and National Center for Atmospheric Research (NCAR). The reanalyzed fields provide global coverage but are of uncertain reliability because of the effects on evaporation of an artificial surface moisture source from a damping term in the reanalysis climate model (Roads et al. 1999), the general mismatch in spatial scales between precipitation observations and the grid scale of the reanalysis (Janowiak et al. 1999), the difficulty in representing precipitation and evaporation (Berbery et al. 1999) accurately in global-scale models, and the fact that the reanalysis did not directly incorporate observations of either precipitation or evaporation (Janowiak et al. 1999). Overall, however, the fields provide a global-scale, globally consistent depiction of the surface moisture fluxes

during the last 51 yr that is useful for the comparisons presented here.

3. Stream flow seasonality

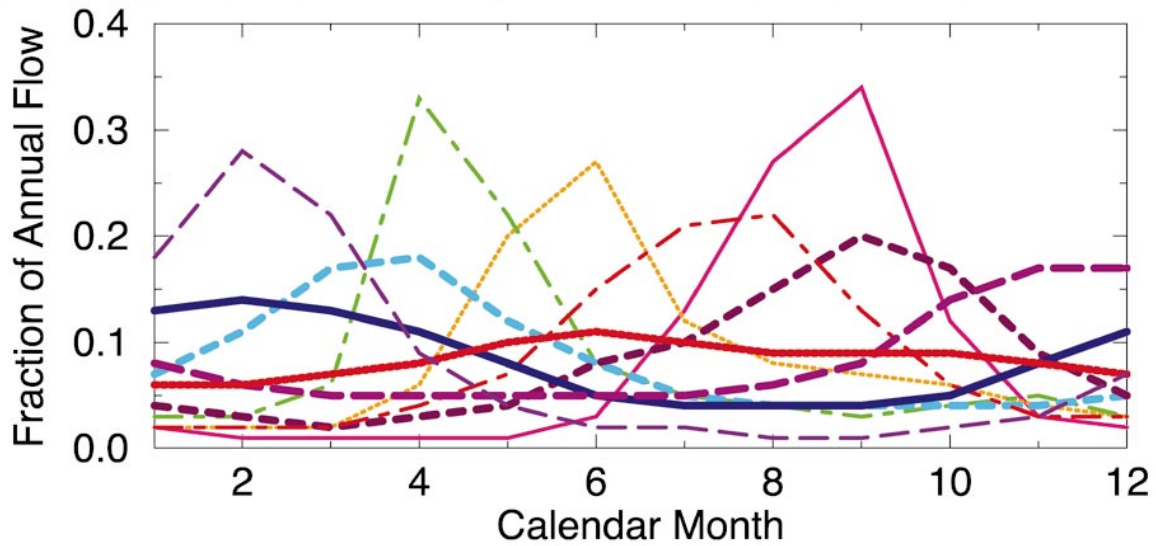
The seasonality of stream flow varies widely from river to river and is influenced mostly by the local seasonal cycle of precipitation, the local seasonal cycle of evaporation demand, the timing of snowmelt (if any), travel times of water from runoff source areas through surface and subsurface reservoirs and channels to the stream gauge, and human management. Summer precipitation generally contributes less stream flow than does the same amount of winter precipitation (because of increased evapotranspiration). Thus, not just the timing but the amount of stream flow can depend on, and directly reflect, precipitation timing. Because the seasonality of precipitation, evaporative demand, and, to a lesser extent, the contributions of snowmelt commonly are large-scale features, stream flow seasonality also exhibits large-scale variations. Because hydrologic channel and basin characteristics, travel times, human influences, and snowmelt contributions have notable local variations, however, there also are many more exceptions to the large-scale patterns of stream flow seasonality than are found, for example, in the spatial patterns of precipitation seasonality.

A global assessment of the geographic distributions of mean annual hydrographs was obtained by a combination of two cluster analyses. These analyses were focused on the climatological fractional monthly flows (CFMFs) of the stream flows, which are the mean monthly percentages of annual flow associated with each month of the year at each of 1137 sites that had suitable records for at least 48 months. A cursory clustering was obtained, first, by Varimax rotation (Richman 1986) of the right-hand vectors from singular value decomposition (SVD; Press et al. 1989) of the matrix of CFMFs, in an extension of the procedure applied to precipitation variability by Logue (1984) and Diaz et al. (1998). The matrix of CFMFs \mathbf{F} had dimension 12 months \times 1137 stations, and the 12 resulting right-hand vectors form a complete, orthogonal basis for decomposing the CFMFs. The right-hand vectors are closely related to the eigenvectors of the matrix $\mathbf{F}\mathbf{F}^T$, where superscript T indicates matrix transpose. Consequently the right-hand vectors are essentially empirical orthogonal functions that provide a way to describe the shapes of mean annual hydrographs at all the sites in terms of a linear sum of the fewest patterns.

The four dominant modes of stream flow seasonality identified by this rotated SVD, not shown here (for brevity and because they largely are represented in Fig. 3b), captured a total of 70% of the global variance of stream flow seasonality. These modes can be described as

- 1) a late boreal spring stream flow maximum across the Timansky and Ural Mountains in Russia, along the

a) Average Fractional Monthly Flows in Kmean Clusters



b) PEAK MONTH IN K-MEAN CLUSTERS

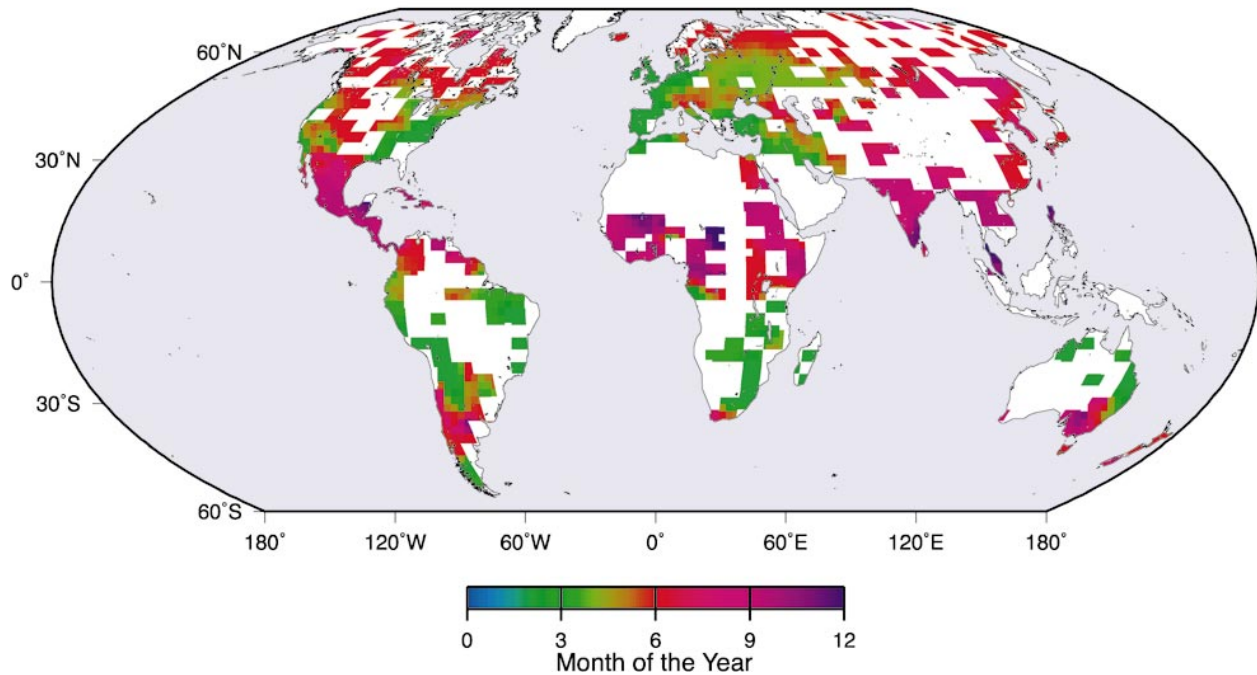


FIG. 3. *K*-mean clusters of climatological fractional monthly stream flows: (a) average fractional monthly flows by month for leading clusters, and (b) distribution of sites in the clusters, with cluster indicated by the peak month in (a).

- southern edge of Siberia (where rivers drain northward from the highlands farther south), and in parts of mountainous southwestern North America (capturing 27% of seasonality variance);
- 2) and 3) two monsoonal mid- to late-summer stream flow modes, one earlier (centered on July–August) and incorporating rivers in the Indian subcontinent, eastern Africa (including parts of the Nile basin), and Sahelian western Africa (capturing 18% of seasonality variance), and the other slightly later (centered on September) and incorporating rivers from tropical West Africa, Central America, and the subtropics of western North and South America (capturing 22% of seasonality variance); and
 - 4) boreal winter-to-spring stream flow maxima toward the headwaters of the first mode (above) in Asia with

TABLE 1. Number of streams in 10 *K*-mean clusters of climatological fractional monthly flows.

Peak month of flow	Curve in Fig. 3a	Color of curve	No. of streams	Fraction of variance
Feb	Light long dashes	Indigo	69	9%
Feb	Heavy solid	Blue	175	8%
Mar–Apr	Heavy short dashes	Turquoise	129	7%
Apr	Light dot–dashes	Green	68	11%
Jun	Light dots	Orange	142	17%
Jun	Heavy dots	Red	262	9%
Jul–Aug	Light dot–dashes	Red	115	11%
Sep	Light solid	Magenta	79	14%
Sep–Oct	Heavy short dashes	Maroon	139	8%
Nov–Dec	Heavy long dashes	Violet	51	7%

some contributions from the Great Lakes region of North America (capturing another 13% of seasonality variance).

A *K*-mean cluster analysis (Hartigan and Wong 1979), initiated from the leading SVD components, provided an alternative regionalization of the “shapes” of mean monthly stream flow hydrographs that specified, for each river, membership in one particular cluster of rivers with similar hydrograph shapes. Thus, the *K*-mean clusters were somewhat easier to visualize than the rotated SVD vectors and will be shown here. All 12 of the unrotated right-hand vectors from the preceding analysis were used as initial conditions for a *K*-mean cluster analysis of the CFMFs. The *K*-mean clusters are delineated so that the CFMFs of all rivers are closest to the mean location, in 12 space, of the elements in the cluster to which they are assigned.

The spatial distribution of the resulting clusters is suggested by Fig. 3b, in which clusters have been categorized by the month of peak flows (Fig. 3a). Their sizes and explained variances are listed in Table 1. Notice that one cluster associated with September peaks has (on average) little flow in other months (light solid magenta curve in Fig. 3a); members of this cluster are located mostly in the subtropical regions (magenta areas in Fig. 3b) where monsoon precipitation induces large amounts of runoff in boreal autumn with low flows during much of the rest of the year. Another cluster with peak flows in April (dot–dashed green curve in Fig. 3a and near the red-to-green transitions in Fig. 3b) also is characterized by low flows through much of the year; members of this cluster are located through the southwestern United States, eastern Europe, and westernmost Asia. These hydrographs mostly reflect northern spring-rainfall- and snowmelt-dominated rivers and regions with pronounced flow effects from the seasonality of evaporation (more discussion on this effect later). A cluster associated with hydrographs that peak near June (heavy dotted red curve in Fig. 3a and red in Fig. 3b) is characterized by nearly uniform flows through most of the year and incorporates stations in the low-altitude, high-latitude regions. Another cluster of rivers peaking

in July (Table 1 and the light dotted orange curve in Fig. 3a) represents seasonal flows that are more concentrated in the early boreal summer, reflecting rapid snowmelt peaks, for example, as in the high-altitude basins of the western United States and in northeasternmost Europe. Notably, clusters in North America and Asia are more smoothly varying and of larger spatial scales than are the clusters of rivers in the tropical and southern continents. The seasonal movements of zonally narrow tropical climatological features, such as the tropical convergence zones (Hastenrath 1996), evidently result in large seasonality gradients through the tropical continents.

Some of the stream flow seasonality regions defined by these cluster analyses reflect regional variations of precipitation seasonality. Among the stream flow regions that correspond directly to precipitation timing are bands of regions across the Tropics in both hemispheres and Australia. Stream flow timing on the northern landmasses is commonly less closely tied to precipitation timing, because stream flow timing variations from region to region may be affected as much by evaporation and topographic and latitudinal influences (on snowpack formation and snowmelt timing) as by precipitation timing.

Simpler measures of stream flow seasonality help to clarify the global mix of seasonal cycles. First, as the simplest index of stream flow seasonality, we can obtain essentially the same patterns as shown in Fig. 3b by mapping the peak month in annual cycles of flow fitted to the period of record at each site. Sine and cosine curves with periods of 1 yr were fitted to each monthly mean stream flow series by simple regressions, and the resulting regression coefficients were used to estimate the phase angle of the annual cycles. The geographical distribution of peak months of annual stream flow cycles characterized this way is summarized in Fig. 4; alternatively, mapping just the month with largest flow in each river’s long-term seasonal cycle yields yet another derivation of essentially the same map. Figures 3b and 4 are in general agreement except in the Rocky Mountains region and in eastern–northeastern Europe. Hydrographs in those areas are characterized by highly concentrated and interannually variable spring snowmelt peaks with low flows in much of the rest of the year. Typically, the hydrographs may have high flows in only one or two months per year; the months in which those high flows occur typically can vary by two to three months from year to year. The simple sinusoidal measure of seasonality used in Fig. 4 is not a very effective representation of hydrographs of this shape and variability, and thus the stream flow timing in these areas is represented better by Fig. 3b than by Fig. 4. Even in Fig. 3b, however, these rivers were parsed to the heavy dotted red curve in Fig. 3a, in which the year-to-year variations in timing of snowmelt results in a flat average hydrograph.

In agreement with continental- and ocean basin-scale

PEAK MONTHS IN MEAN STREAMFLOW CYCLES

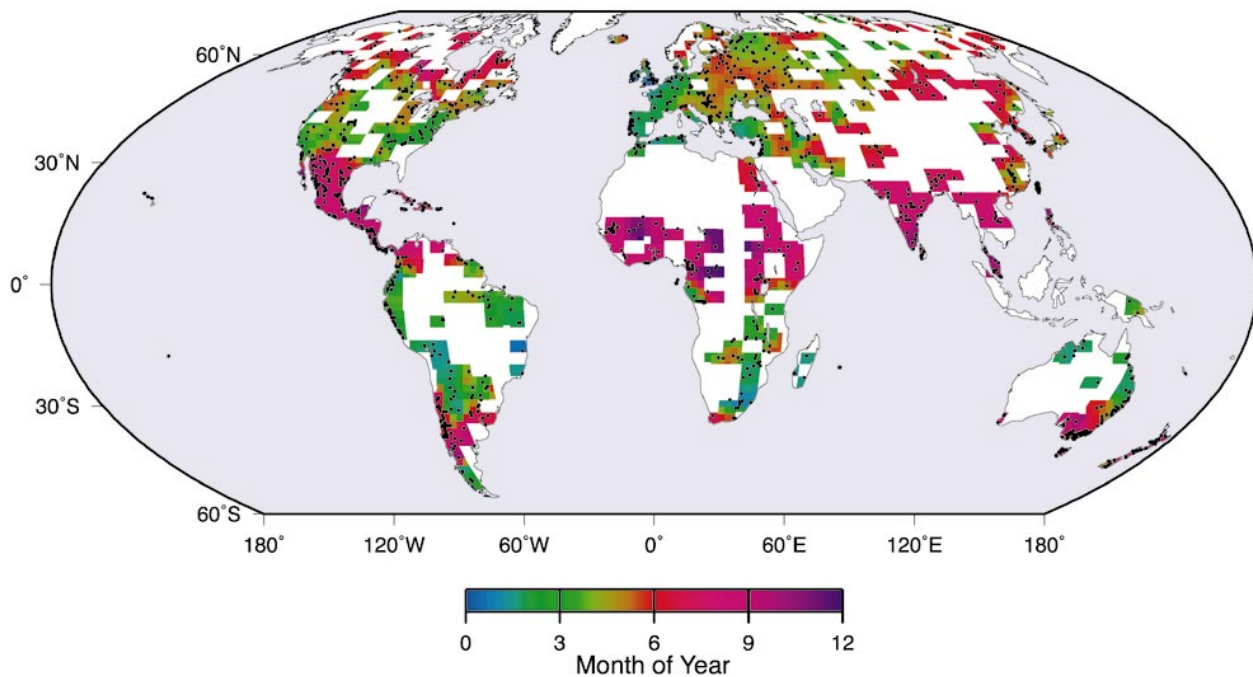


FIG. 4. Peak months in simple annual cycles of stream flow. Shading interpolates between mean peak months for streams within $2^\circ \times 2^\circ$ grid cells, where available, with color scheme indicated at bottom; sites used indicated by black dots. Annual cycles are fitted to stream flow series with at least 48 months of record, by method outlined in text.

averages estimated by Korzun (1978), European rivers and rivers in much of midlatitude North America have seasonal peak flows in boreal spring. North American rivers draining to the Arctic peak in boreal summer. Central American rivers peak in boreal autumn when monsoon precipitation and tropical storms are active. Asian rivers overall tend to peak in boreal summer and autumn except in the far west. Western African rivers draining to the tropical Atlantic peak mostly in mid- to late boreal autumn; rivers draining to the Indian Ocean tend to peak in boreal winter and spring. A relatively strong gradient in the timing of seasonal flows characterizes stream flows along, at least, the eastern coast of Australia, and flow seasonality varies considerably from region to region within South America depending on whether runoff sources are in the Andes or in various lowlands.

Runoff rates per unit area are correlated marginally with the month of peak flows (correlation coefficient $r = +0.08$), as a result, at least, of some of the larger river systems—most notably the Nile—that exhibit later seasonal peaks as sites farther and farther down the river are considered. (As with the other correlations reported in this paper, the present dataset contains many sites— $n = 962$ in this case—for the statistical analysis. Redundancies associated with sites that measure stream flow downstream from other sites in the dataset reduce the degrees of freedom by one-quarter, so that there are effectively about 719 degrees of freedom. Consequently,

the significance level for this correlation is $p = 0.03$, by a simple t -statistic test of a null hypothesis of $r \neq 0$. More important, however, the amount of variance explained by the association, $r^2 = 0.0036$, is very small.)

To understand the distributions of stream flow seasonality among and within the continents, consider that, globally, the peak months in the fitted annual cycles vary from river to river, in very general terms, from maximum flows in the local warm season in some of the highest latitudes, to northern winter and spring in the midlatitudes, to local autumn in the subtropics and parts of the Tropics. The coincidence of maximum temperatures and maximum flows in the high latitudes reflects the release of water from snowpacks and ice. Mid-latitude stream flow seasonality in many areas, such as most of North America and western Russia, is determined by the influences of winter maxima for precipitation and winter minima for evapotranspiration, and by the persistence of any snowpacks that feed the streams. Elsewhere in the midlatitudes, summer or autumn precipitation maxima establish summer or autumn stream flow maxima. The autumnal peak flows in many subtropical and (less so) tropical rivers reflect arrival of, and runoff from, monsoon rains. The equatorward transition from winter-supplied runoff to monsoon-supplied runoff is particularly notable in the rivers of North America and Australia. Similar patterns of stream flow “seasonality” were found when the month with the peak

flow rates among each river's period-of-record mean monthly flow hydrographs was mapped (not shown) instead of the peaks of fitted sines and cosines; a more complex cluster analysis of stream flow seasonality earlier in this section also delineates essentially the same patterns.

Because much of the character of the stream flow hydrographs is derived from the timing of precipitation and evaporation within the year, it is useful to consider the geographic distribution of lags between seasonal cycles of precipitation, precipitation minus evaporation, and stream flow. The lags between peak months in the period-of-record annual cycles of precipitation (determined by the same method used and described previously for stream flow) and stream flow are shown in Fig. 5a, from a comparison of the global stream flow dataset and the gridded mean precipitation of Eischeid et al. (1995).

Lags between peak precipitation month and peak stream flow month vary from long delays in high latitudes and mountainous regions to relatively short delays (0–3 months) nearly everywhere else; overall, the correlation between lag and latitude in the dataset is $r = +0.27$ ($p < 0.001$), but, in midlatitudes, the relation is stronger for many rivers. There are many local exceptions to this pattern, but, on large scales, it corresponds to long delays between snowfall and the melting of snow and ice at the high latitudes and in the basins draining the American cordillera, grading toward short (1–3 month) lags between the peak precipitation month and peak flow months through most of the lower-altitude midlatitude and tropical lands. This spatial pattern is simpler than the patterns of peak flow months in Figs. 3b and 4, because the complex patterns of precipitation seasonality have effectively been removed. Although stream flow series, and parts of series, that showed obvious changes in stream flow timing and variability were culled from the dataset, more subtle reservoir effects also may be contributing to stream flow lags in some rivers. Globally, though, logarithms of the basin areas are correlated with the lag between precipitation- and stream flow peak months ($r = +0.18$, $p < 0.001$) but do not capture much of the overall variance.

The lags between precipitation peaks and stream flow peaks are notably long in the eastern United States and eastern Europe (Fig. 5a). In these areas and other areas, stream flow seasonality is more a function of the winter–spring evaporation minimum than of precipitation timing. As a consequence, lags between the seasonal maxima of precipitation minus evaporation (Kalnay et al. 1996) and stream flow in the eastern United States and eastern Europe (Fig. 5b) are considerably shorter than the lags between precipitation and stream flow (Fig. 5a). Elsewhere, differences between Figs. 5a and 5b are modest, indicating that precipitation timing is the more common control on stream flow timing. Globally, basin areas and the lags between precipitation minus evaporation and stream flow are uncorrelated ($r = -0.01$, p

$= 0.77$), and, although statistically different from zero, the correlations between these lags and mean precipitation minus evaporation are not substantially more explanatory ($r = +0.13$, $p < 0.001$).

Mean monthly flows may vary dramatically from month to month in some regions, whereas, in others, flows vary only modestly from month to month. Overall, hydrographs vary from having most flow in a single month or season to having nearly uniform flow throughout the year, depending, under natural conditions, on factors such as the distribution of precipitation within the year, the extent to which evapotranspiration seasonalities modify flow rates, the extent to which runoff “accumulates” in snow and ice, and the smoothing influences of some long and tortuous river networks and aquifers. Shown in Fig. 6 is the global pattern of the percentage of annual stream flow occurring during the month of the year with maximum flows among the period-of-record mean monthly flow rates. The bluer colors indicate more uniform long-term mean hydrographs and redder colors indicate more steeply peaked hydrographs. Most notable on a global scale are the relatively uniform flows of major tropical rivers, indicated by peak flow percentages near 10%, and the sharp peaks in Siberian and in monsoonal and subtropical rivers of southwestern United States and Mexico, Africa, Australia, India, and Chile, indicated by peak flow percentages near 50% (see also Korzun 1978). In the midlatitudes, wetter climates (e.g., eastern United States and Europe) commonly yield more uniform stream flow hydrographs than do drier climates. Globally, the percentages of flow in the peak months do not vary directly with basin area, but rather, in this dataset, there is a tendency for the largest and smallest basins to yield more uniform flow seasonality overall, whereas the rivers emerging from basins between about 500 and 10 000 km² yield the whole range of percentages from almost uniform to just a few months with flow. The percentages of flow in the peak month, however, do vary with the amount of runoff per unit area generated in the basins. The inset to Fig. 6 shows, amid considerable scatter, the tendency for the wetter basins to yield more uniform flows ($r = -0.28$, $p < 0.001$), reflecting in part the well-known flashiness of flows in many rivers from semiarid-to-arid basins and the steadiness of flows in rivers from humid basins.

4. Global runoff rates

Average stream flow at a point along a river is the product of the total catchment area above the gauge and the average rate at which runoff is generated from snow and rain in that catchment. Long-term mean runoff rates (stream flow per unit basin area) vary from site to site in the global dataset in response to broad differences in aridity of the regions and in response to contributions from orographic sources. Runoff rates from 969 sites in the dataset, for which basin areas are known and are less than 100 000 km² and which had 48 months or more

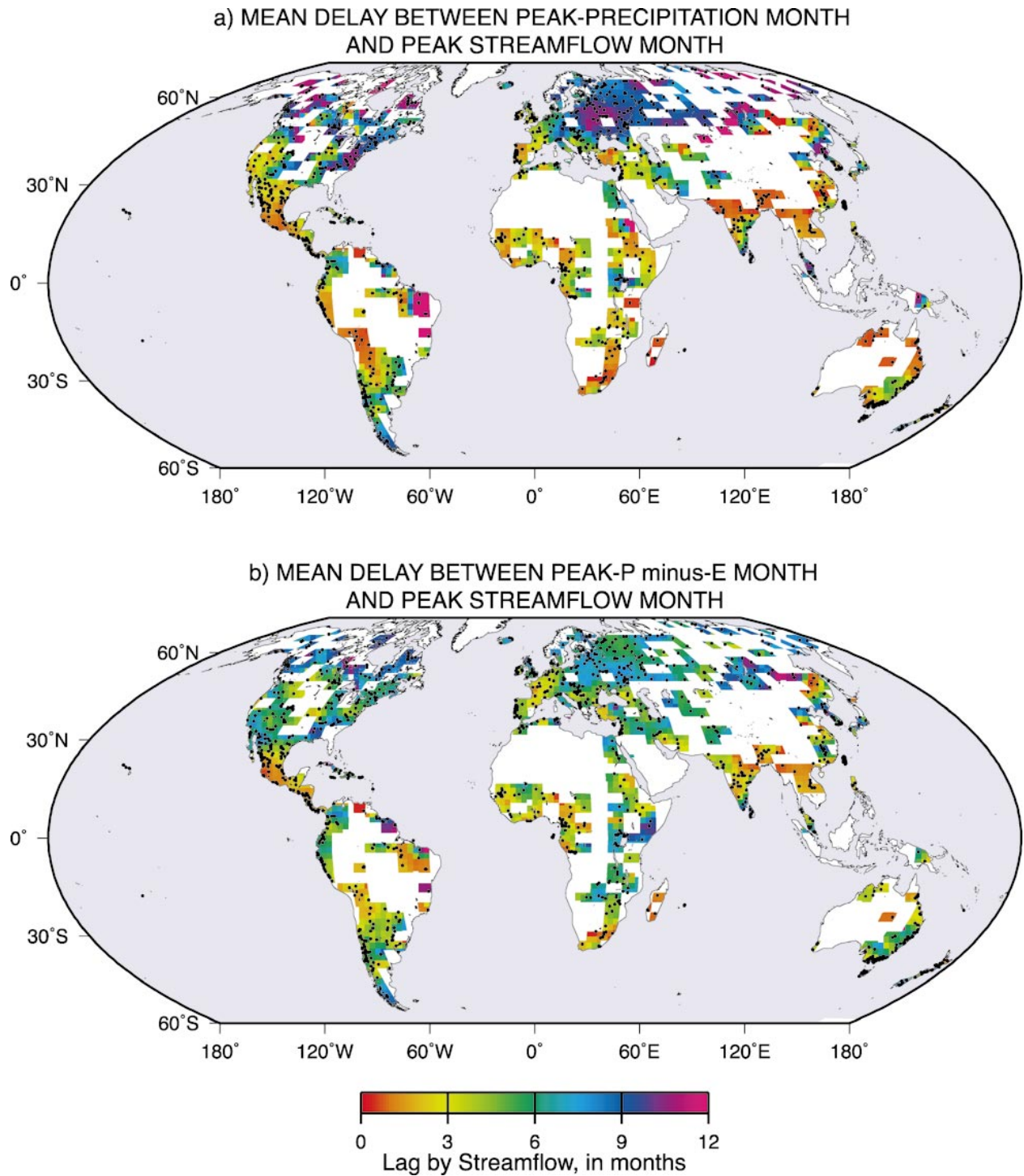


FIG. 5. Mean delay, in months, between peak month in (a) the annual cycle of precipitation and (b) precipitation minus evaporation and the peak month in annual cycle of stream flow. Precipitation averages from grid cells in the Eischeid et al. (1995) global precipitation dataset, within which stream flow series are available, are used to fit precipitation cycles; precipitation-minus-evaporation averages from grid cells in the NCEP-NCAR reanalysis global surface fluxes dataset (Kalnay et al. 1996) are used to fit precipitation-minus-evaporation cycles.

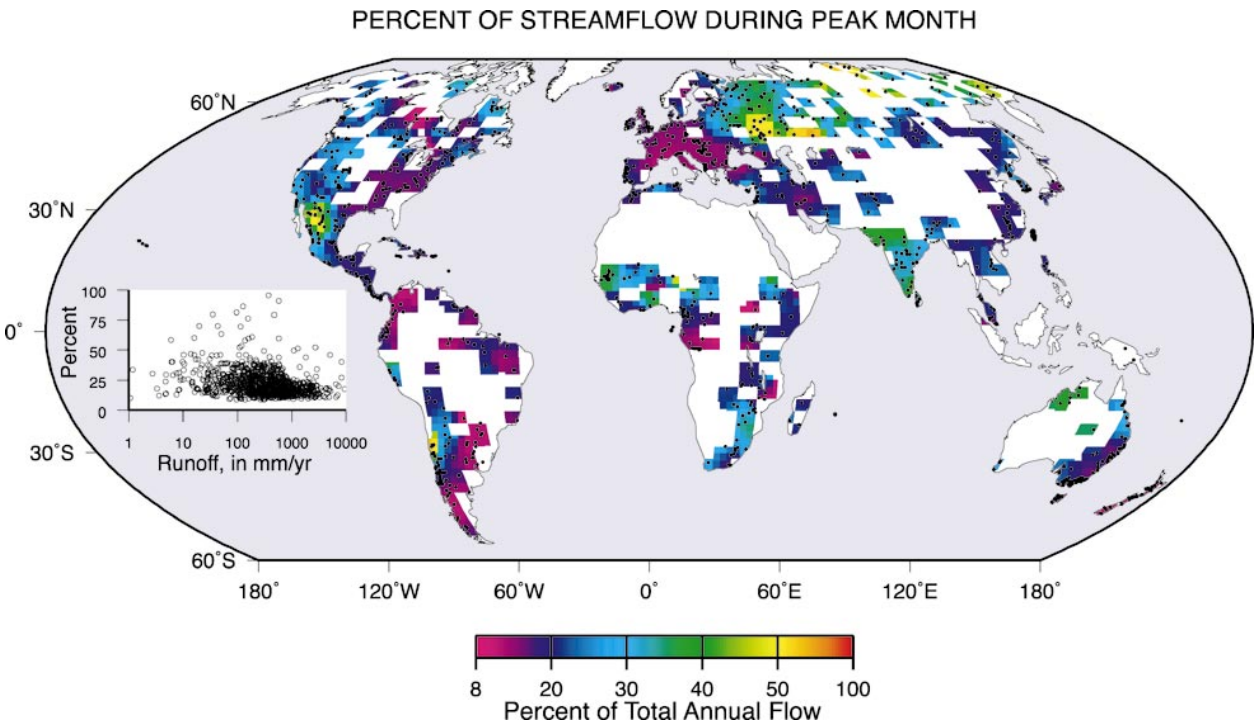


FIG. 6. Period-of-record mean percentages of annual mean stream flow that occur within the month of maximum flow in each river's monthly mean hydrograph. Inset shows relation of percentages to runoff per unit area.

of record, are mapped in Fig. 7. Maximum mean runoff rates are encountered near the tropical western Pacific, where vigorous cumulus convection frequently produces prodigious precipitation totals to supply runoff rates totaling several meters per year in some locations. Comparable runoff rates are found in monsoon regions of northern India [see Korzun (1978) for discussions of comparable mean runoff rates]. A meter or more of runoff is generated annually in some subbasins of the Amazon and Congo and in other tropical rivers. Elsewhere, runoff rates generated in basins of humid northwestern and northeastern North America and northern Europe are high relative to many other extratropical settings. Low runoff rates (on the order of a few millimeters per year or less) are generated in the southwestern United States, northeastern Mexico, north of the Aral Sea, northeastern China, and southernmost Africa. The lowest runoff rates ($\sim 1 \text{ mm yr}^{-1}$) are found in the Sahel (Fig. 7), with even drier conditions presumed to prevail in the Sahara and Arabia.

Globally, runoff rates vary directly with observed annual precipitation rates ($r = +0.41$, $p \ll 0.001$), as expected from common sense and the preceding discussion of Fig. 7. We thus are concerned to report that mean runoff rates are less closely correlated ($r = +0.20$, $p < 0.001$) with the NCEP–NCAR reanalysis annual precipitation-minus-evaporation totals, although the relationship is still statistically significant. As noted in section 2, both precipitation and evaporation estimates in the NCEP–NCAR reanalysis (Kalnay et al. 1996) are

considerably removed from the observational record and thus retain notable biases (e.g., Roads et al. 1999; most recently, Maurer et al. 1999) that may be degrading their relation to the stream flow records studied here. In addition to these broad regional climate influences, globally, the calculated runoff rates tend to decrease with increasing $\log(\text{basin area})$: see the inset to Fig. 7 ($r = -0.32$, $p < 0.001$). These decreases reflect the greater proximity to the runoff-generating wet catchments in most smaller river basins and the greater opportunities for evaporative and other losses during transit through many large basins (Kalinin 1971).

The runoff rates shown in Fig. 7 are comparable to regional rates estimated by Baumgartner and Reichel (1975) and are, of course, in agreement with local studies (from which many of the stream flow data and basin areas were obtained). On a global scale, average runoff rates were calculated for each 5° -lat band from 40°S to 55°N , and are shown in Fig. 8b, along with zonally averaged ratios of runoff to precipitation (Fig. 8a), also presented in map form in Fig. 9. A tropical maximum runoff rate associated with rivers in the tropical western Pacific islands and with the southern Amazon basin dominates the zonal runoff distribution, along with maxima associated mostly with high runoff rates from basins in the highlands of the subcontinent, from the Andes, and in New Zealand (near 40°S). Subtropical runoff minima also are evident but probably are underrepresented here (i.e., values are overestimated), because stream flow records are not available from some of the

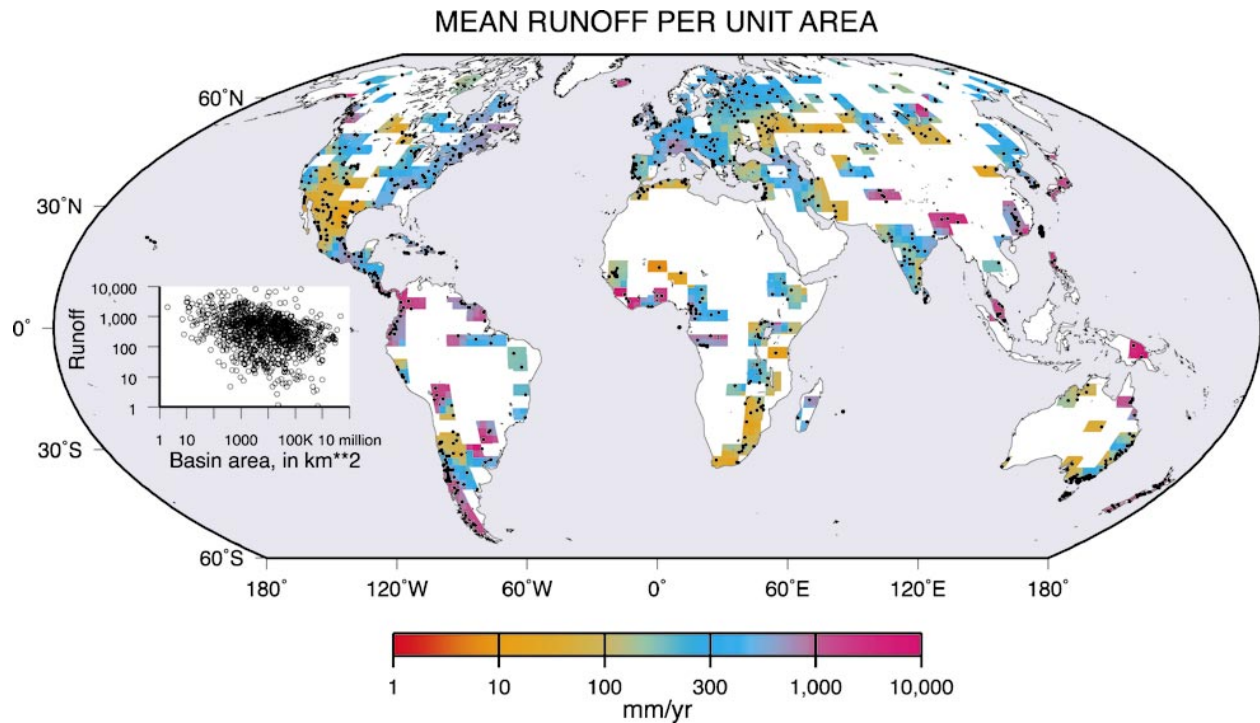


FIG. 7. Period-of-record mean runoff rates (as the mean annual stream flow per basin area); shading represents a smoothing between mean runoff rates for sites within $2^{\circ} \times 2^{\circ}$ grid cells and has been stretched between 100 and 1000 mm yr^{-1} to emphasize the most populous range. Inset shows relation between runoff rates and basin areas.

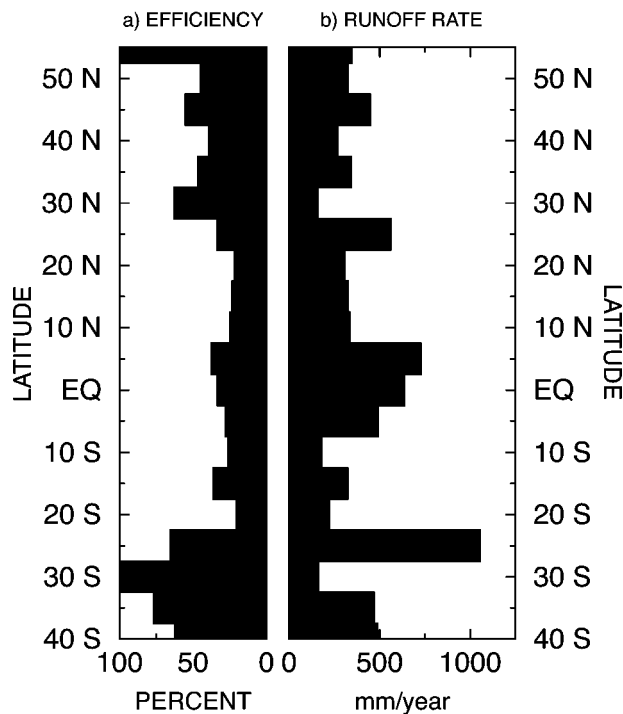


FIG. 8. Averages of (a) period-of-record mean runoff efficiencies and (b) period-of-record mean runoff rates from 833 stream flow sites, in 5° -lat zones. Efficiencies (runoff per unit area divided by precipitation per unit area) are calculated as discussed in text and the caption of Fig. 9.

largest desert areas (Sahara, Arabia, parts of South Africa, and central Australia). Also the subtropical runoff “minimum” in the Northern Hemisphere is interrupted by the monsoon-driven maximum near 25°N . These broad runoff distributions are in qualitative agreement with the estimates developed by Baumgartner and Reichel (1975; see also McMahon et al. 1992). The locations of extratropical peaks and troughs in the figure align qualitatively with latitudinal water budget surpluses estimated by Legates and Mather (1992).

Integration of the runoff rates over the 5° -lat bands of Fig. 8 yields a land area-weighted average runoff rate of 404 mm yr^{-1} . This estimate is in reasonable agreement with the mean areal runoff rates of 410 and 540 mm yr^{-1} of McMahon et al. (1992) for basins between 10^3 and 10^5 km^2 . Both this estimate and McMahon et al.’s, however, are based on a sampling of only a fraction of the global land surfaces (22% in this case) and on samplings that are biased against some of the driest areas. The current estimate thus is useful mostly as a measure of the global representativeness of the dataset. The weighted estimate is much larger than Baumgartner and Reichel’s (1975) estimated global-average land runoff rate of 266 mm yr^{-1} . Their runoff totals, however, are based on estimates of precipitation minus evaporation and are not directly comparable with either McMahon et al. (1992) or the observations used here. Their estimates, for example, include broad desert regions with negative “runoff.” Overall, then, the cur-

MEAN RUNOFF EFFICIENCY (Runoff/Precipitation)

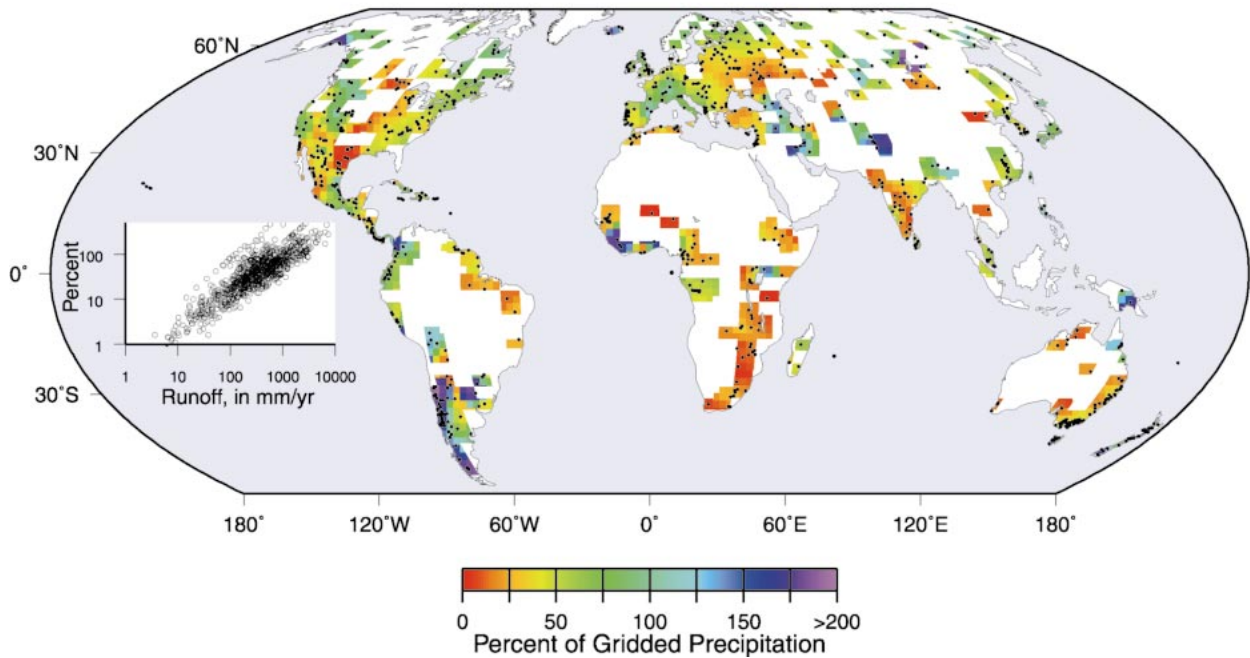


FIG. 9. Period-of-record mean runoff efficiencies, defined as mean runoff rate divided by mean precipitation rate; shading represents a smoothing between $2^{\circ} \times 2^{\circ}$ grid cell mean runoff efficiencies. Inset shows relations between runoff efficiencies and runoff rates. Mean precipitation rates used are from the precipitation averages of the $5^{\circ} \times 5^{\circ}$ cell in Eischeid et al. (1995) that encloses the stream flow site.

rent runoff estimate is in agreement with other stream flow–based estimates but may overestimate the true global average.

The average precipitation rate in those $5^{\circ} \times 5^{\circ}$ grid cells of the Eischeid et al. (1995) precipitation dataset that coincide with sites in the stream flow set is 1087 mm yr^{-1} . Thus, average runoff is about 41% of corresponding land precipitation, which is in close agreement with the global estimate that 39% of precipitation runs off from land to oceans made by Baumgartner and Reichel (1975). Although only 22% of land surfaces are represented in the global stream flow dataset, the distribution of sites is evidently sufficiently widespread that global runoff processes are reasonably well recovered in the largest-scale average. This fact is also evidenced by the observation that the subsample of $5^{\circ} \times 5^{\circ}$ gridded precipitation used is in close agreement—within 1%—with the full global land average precipitation rate in the Eischeid et al. (1991) dataset.

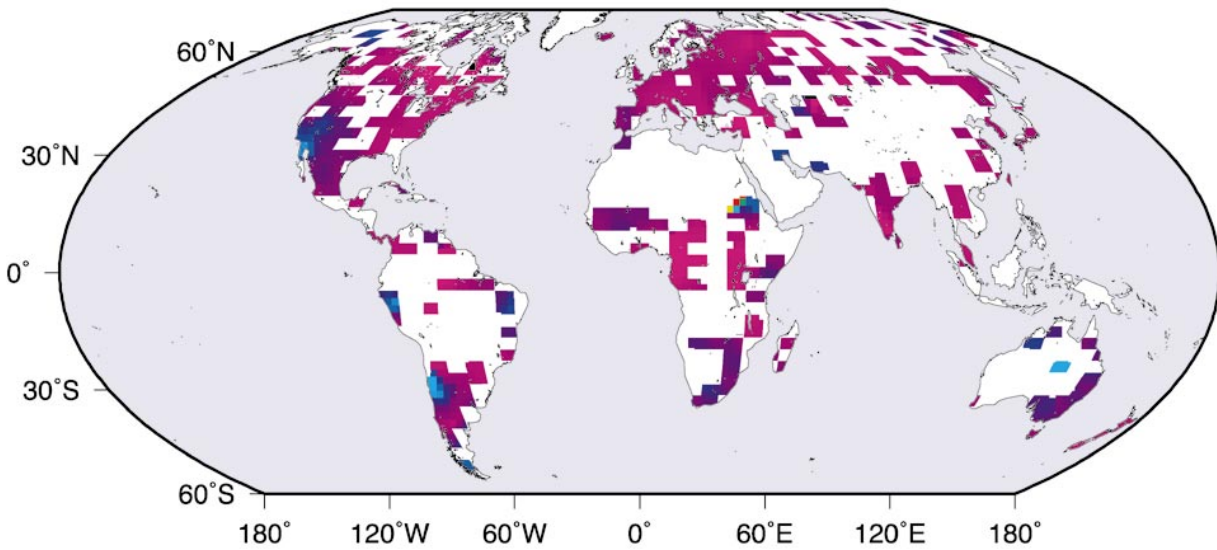
The ratios of long-term runoff rates to mean precipitation rates vary dramatically from region to region, as shown in Fig. 9. The ratios plotted in Fig. 9 range from virtually zero in the northern Sahel to over 100% in river basins fed by mountainous or very humid terrains. Low ratios (runoff efficiencies) are found through broad semiarid-to-semihumid regions of North America and Asia, in the eastern Amazon basin, in much of Africa (excepting only tropical western Africa), and in northernmost Australia. High ratios of runoff to precipitation

occur at mostly higher, cooler latitudes and in extremely humid regions (Fig. 8a). Ratios over 100% result from measurement biases or from mismatches between the observed stream flows and the large-scale gridded precipitation averages assumed to feed them. Many of the gridded precipitation rates are low-altitude biased and much less than the high-altitude precipitation rates that provide most of the runoff; for rivers that drain some of the highest mountain basins, for example, rivers in western North American and, especially, the southern Andes, consequently, the ratios plotted in Figs. 8a and 9 for these basins are unrealistically large. Globally, the relationship between runoff efficiency and runoff rate (as a measure of aridity of the river basins) is very strong (see inset to Fig. 9; $r = +0.87$, $p \ll 0.001$). The logarithm of basin area is somewhat less correlated with the runoff efficiencies ($r = -0.29$, $p < 0.001$), with the largest basins suffering the largest evaporative losses and thus the lowest efficiencies.

5. Year-to-year stream flow variability

Year-to-year variations in stream flow play an important role in the development and management of water resources in most regions. For 858 sites with 10 or more years of stream flow data, the (unweighted) average coefficient of variation is 49%; this coefficient is the ratio of the standard deviation of annual flows to the mean annual flow. The global distributions of co-

a) COEFFICIENTS OF VARIATION OF ANNUAL PRECIPITATION



b) COEFFICIENTS OF VARIATION OF ANNUAL STREAMFLOW

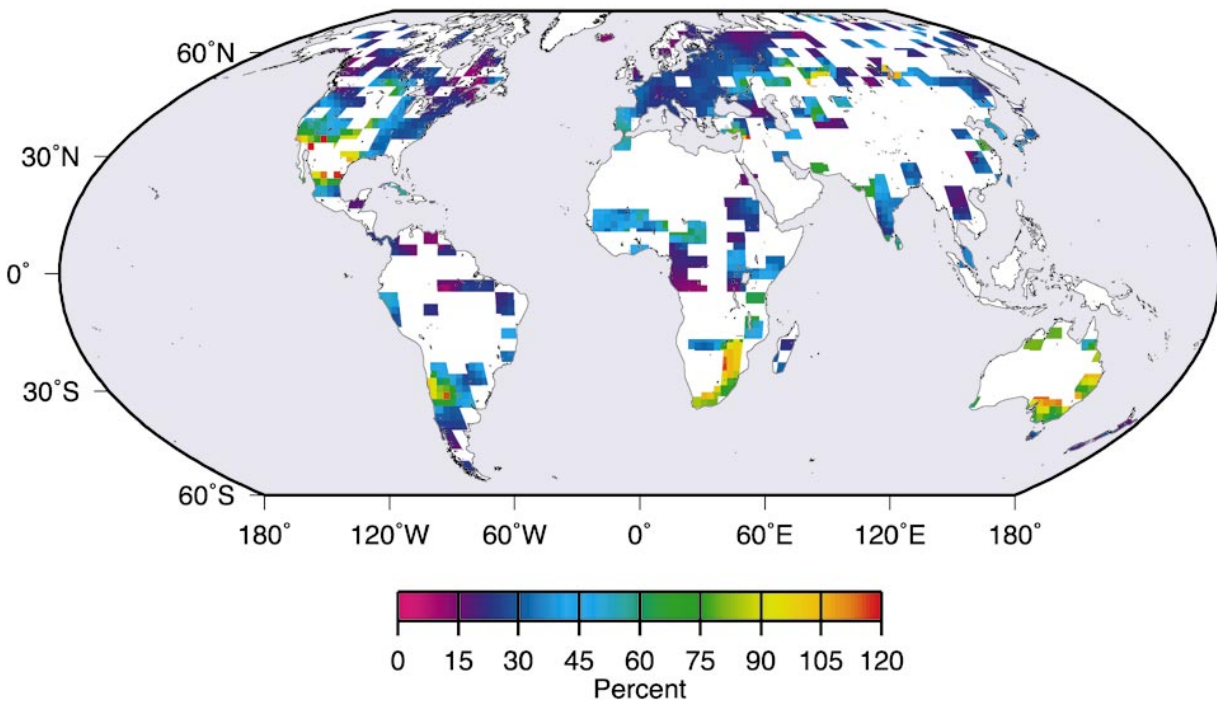


FIG. 10. Coefficients of variation of annual (a) precipitation and (b) stream flow totals during years with stream flow record (in rivers with 10 yr or more of record). Precipitation totals are from those $5^{\circ} \times 5^{\circ}$ grid cells in the Eischeid et al. (1995) precipitation dataset that contain stream records.

efficients of variation of annual precipitation and stream flow are mapped in Fig. 10. Stream flow coefficients of variation (Fig. 10b) clearly are much larger than are the corresponding variations of precipitation (Fig. 10a) in most regions. Overall, the average coefficient of vari-

ation of precipitation—in those $5^{\circ} \times 5^{\circ}$ precipitation grid cells from Eischeid et al. (1995) that are occupied by stream flow sites—is only 12%. Similarly, McMahon et al. (1992) report smaller coefficients of variation for precipitation than for runoff, averaging about 0.2 for

precipitation and 0.6 for runoff. Although soil moisture and other integrating influences within river basins typically reduce the shortest-term variations of rivers relative to their precipitation sources on timescales much less than annual (e.g., Changnon 1987), the nonlinear linkage between overall sources and sinks on annual and longer timescales yields stream flow variations that are larger (in relative terms) than the precipitation and evaporation fluctuations that force them. For example, whether by flood or by snowmelt, stream flow responses to precipitation generally are more brief and intense than the time intervals during which evaporation can influence the flows; this fact leads to the common condition that rainy periods yield disproportionately more runoff and droughts yield disproportionately less runoff than might be expected from the corresponding annual precipitation variations.

In Fig. 10, the cooler and wetter regions, such as the far northern lands and the tropical rivers of South America and Africa, typically exhibit interannual flow variations that are small in comparison with the mean annual flows, yielding small coefficients of variation. Drier settings in the North American Southwest, Chile, the Sahel, South Africa, and Australia exhibit relatively larger interannual variations (yielding large coefficients of variation, with standard deviations that are 60%–100% or more of the long-term means). These rivers typically have small base flow rates that persist throughout much of the year, with just a few large but brief floods that determine much of the annual total flow in a given year. Globally, the coefficients of variation of precipitation and runoff are modestly correlated ($r = +0.23$, $p < 0.001$). The coefficient of variation of runoff is anticorrelated with average runoff ($r = -0.47$, $p \ll 0.001$), however, which is similar to the correlation value between the coefficient of variation of precipitation and mean precipitation ($r = -0.46$, $p \ll 0.001$). The coefficient of variation of runoff is significantly correlated with $\log(\text{basin area})$ in this global collection of rivers ($r = -0.09$, $p = 0.002$) but without much explanatory power.

These year-to-year variations can be broken down into short-term interannual fluctuations and longer decadal variations. The fractions of the overall variances of annual stream flow and gridded precipitation series that remain in high-pass-filtered versions of the same are shown in Fig. 11. The series were high-pass filtered to retain interannual frequencies higher than $(7 \text{ yr})^{-1}$, that is, with timescales less than 7 yr. This division of variance around a $(7 \text{ yr})^{-1}$ frequency is somewhat arbitrary but is designed to fall near the low-frequency end of the spectrum of tropical climate variations associated with El Niño events and near the high-frequency end of the decadal and interdecadal climate variations of the North Pacific and Atlantic climate systems (Cayan et al. 1998; Dettinger et al. 1998, 2000a). Overall, the relative contributions of interannual variability to precipitation and stream flow variability are very sim-

ilar (e.g., the mean precipitation variance fraction in Fig. 11a is 69% and the mean stream flow variance fraction in Fig. 11b is 61%).

Larger components of decadal stream flow and precipitation variation, indicated by cooler colors (violet), are found in rivers in Canada, Argentina, and Brazil, and in much of tropical Africa. Warmer colors indicate rivers that have larger components of interannual variability. Tropical rivers of South America and Australia have relatively large components of interannual variability, as do rivers in the North American Southwest and central Asia. Many of the rivers with enough continuous record to test have nearly equal contributions from interannual and decadal frequency ranges (greens).

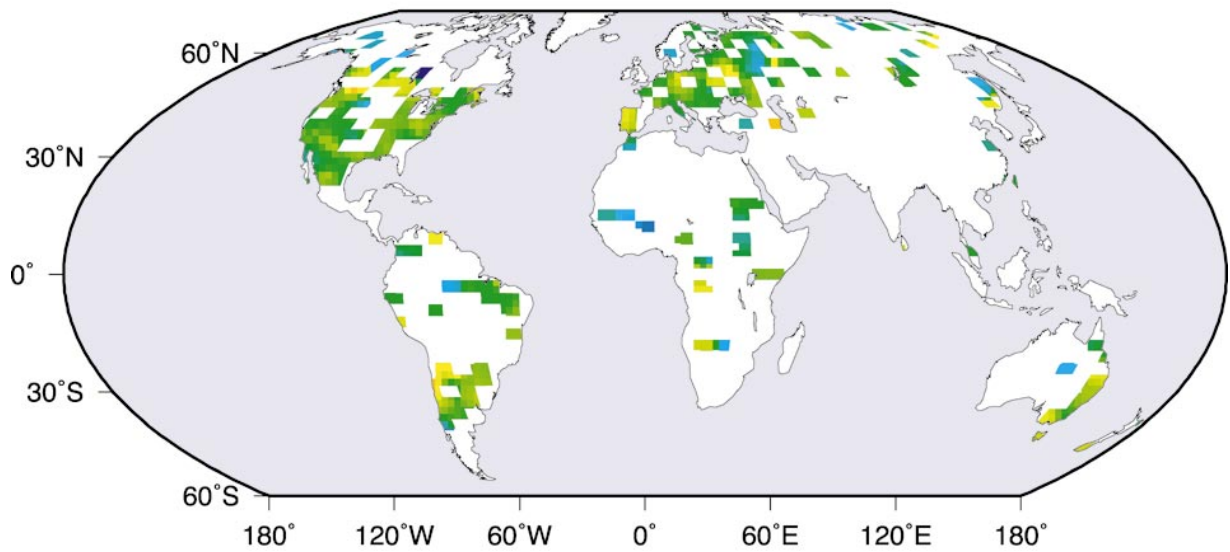
Globally, the fractions of high-frequency variance in precipitation and stream flow are modestly correlated ($r = +0.22$, $p < 0.001$), and there are clear instances in Fig. 11 of coincidences between large (or small) fractions of high frequency in both precipitation and stream flow (e.g., most notably, in the Sahel). Overall, the fractions of high-frequency variance in precipitation and stream flow depend only moderately on the mean precipitation and runoff rates (e.g., correlation between high-frequency fraction of stream flow variance and mean runoff is $r = +0.18$, $p = 0.002$). On a global basis, the high-frequency fraction of stream flow variance is, instead, best related to area [correlation with respect to $\log(\text{area})$ is $r = -0.45$, $p \ll 0.001$]. The relatively strong negative association between basin area and high-frequency stream flow variance may be due to the larger natural reservoirs and thus larger capacities for forms of low-pass filtering in the larger river basins (Yevdjevich 1963), along with more opportunities for human interventions that impart low-frequency changes to the larger river regimes.

These year-to-year stream flow variations commonly have been analyzed and managed as random events either locally or on global scales (e.g., McMahon et al. 1992). Among these variations, however, many are associated with large-scale climatic fluctuations from a variety of sources that vary from region to region. The large scale of these variations (Kalinin 1971; Probst and Tardy 1987, 1989), as well as prospects for predicting future variations from climatic considerations, makes the more structured parts of the stream flow patterns particularly important. Correlations between selected indices of large-scale climatic variability and annual stream flow totals illustrate global teleconnections that result in such flow variations and are considered next.

a. Southern Oscillation index

One of the most widely studied indices of global climate variation is the Southern Oscillation index (SOI), which is the normalized east–west difference in atmospheric pressures along the tropical Pacific (specifically, at Tahiti and Darwin, Australia). SOI is a measure of the atmospheric conditions usually associated with fluc-

a) FRACTION OF INTERANNUAL VARIANCE IN ANNUAL PRECIPITATION



b) FRACTION OF INTERANNUAL VARIANCE IN ANNUAL STREAMFLOW

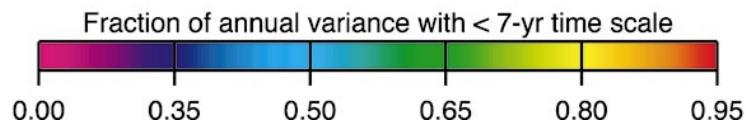
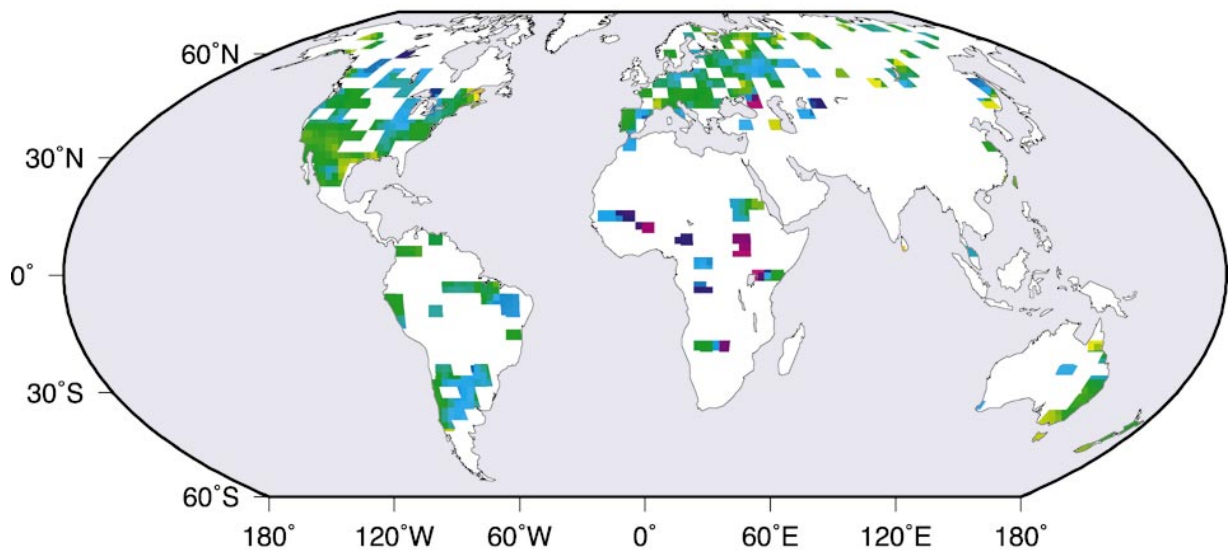


FIG. 11. Fractions of annual variance of (a) precipitation and (b) stream flow from interannual frequencies, greater than $(7 \text{ yr})^{-1}$. Annual flow series in rivers with more than 30 yr of continuous record were digitally filtered (Kaylor 1977) using a high-/low-pass filter with half-power point at $(7 \text{ yr})^{-1}$ to determine these fractions.

tuations between the El Niño warm-temperature phases and the La Niña cool-temperature phases of the tropical Pacific Ocean (Philander 1990). These tropical fluctuations affect temperatures and precipitation in regions all over the globe (Ropelewski and Halpert 1987, 1989,

1996; Kiladis and Diaz 1989). Our purpose here is to illustrate briefly that these large-scale tropical fluctuations yield similarly global-scale influences on stream flow and that stream flow teleconnections are as pervasive as are meteorological teleconnections. A more

detailed characterization of these influences is presented by Dettinger et al. (2000b) at global and hemispheric scales and, at regional scales, by numerous other authors (e.g., Redmond and Koch 1991; Cayan and Webb 1992; Chiew et al. 1994; Eltahir 1996; Guetter and Georgakakos 1996; McKerchar et al. 1996; Piechota and Dracup 1996; Zorn and Waylen 1997).

Correlations between October–September stream flow totals and the December–February SOI (when the El Niño will have reached its fullest development) are shown in Fig. 12a. [Notice that, despite the regional differences in stream flow seasonalities discussed in previous sections, a “water year” from October through September is used here as an arbitrary but familiar time unit. Some of the ramifications of such a choice, for a study of SOI teleconnections in the Western Hemisphere, are illustrated by Dettinger et al. (2000b).] The main regions for which stream flows are significantly correlated with SOI include much of the Americas, Europe, and Australia, mostly in response to changes in precipitation associated with El Niño or La Niña events. During El Niño events, in response to equatorward migration of midlatitude westerly winds, jets, storm tracks, and hence precipitation that occur when SOI is negative, stream flows are generally low in the northwestern and easternmost North America, in tropical Central America, and in South America (Rogers 1988). In response to global-scale changes in patterns of tropical convection and precipitation, stream flows in the Nile basin (Eltahir 1996) and in Australia also are generally low during El Niño events. During El Niño events, large stream flows are typical in subtropical South America, in southwestern North America, and in Europe. Broadly opposite patterns of high and low stream flows occur during La Niña events.

The statistical significance of these correlation patterns was tested by counting the number of sites with “significant” correlations (by t test) that have neighboring sites—within 500 or 1000 km—that are also significantly correlated with SOI; these counts of neighboring correlations were compared with 1000 random distributions of the same number of significant correlations as shown in Fig. 12. The correlation patterns shown in Fig. 12 are more clustered, that is, more geographically coherent, than any of the 1000 random maps, indicating a high level of confidence in the overall importance of the SOI and these global patterns of stream flow correlation.

Mean differences in precipitation between El Niño years and La Niña years, and the corresponding changes in stream flow, are shown in Fig. 13 ($r = +0.75$, $p < 0.001$). In keeping with the larger coefficients of variation of stream flow (in comparison with precipitation) shown in Fig. 10, the flow differences between El Niño years and La Niña years are a much larger (roughly five times larger) fraction of mean rates than are the precipitation differences. Considering all years (not just El Niño and La Niña episodes), McMahon et al. (1992)

show a similar ratio of runoff variations to the forcing precipitation variations of about 3–4. The largest flow differences in Fig. 13, both at positive and negative extremes, are from rivers with large overall coefficients of variation, such as the subtropical rivers of southwestern North America and Australia shown in yellows and reds in Fig. 10. Notice also that all but one of the tropical rivers with significant El Niño minus La Niña flow differences are drier during El Niño years than during La Niña years; the one outlying, positive solid dot in Fig. 13 represents the Paranapanema River in Brazil, which is gauged in the Tropics but drains northward into the Tropics from a basin at the boundary between the Tropics and subtropics. Thus, all the tropical rivers with significant correlations to SOI are drier than normal during El Niños. This El Niño dryness is a reflection of a general wet ocean–dry land condition in the Tropics that is fostered by El Niño dynamics (Diaz 1996; Morrissey and Graham 1996). The average tropical stream flow difference between El Niño years and La Niña years is about -11% to -31% of long-term mean flow (depending on whether rivers with nonsignificant flow differences are included); this difference is forced by precipitation differences of about -9% to -16% . Extratropical differences between El Niño and La Niña stream flow (and precipitation) vary more in magnitude and sign from region to region but tend to average to positive fractions of mean flows globally. Overall, the changes in extratropical stream flows illustrated in Fig. 13 average to $+25\%$ of mean flow and $+12\%$ of mean precipitation.

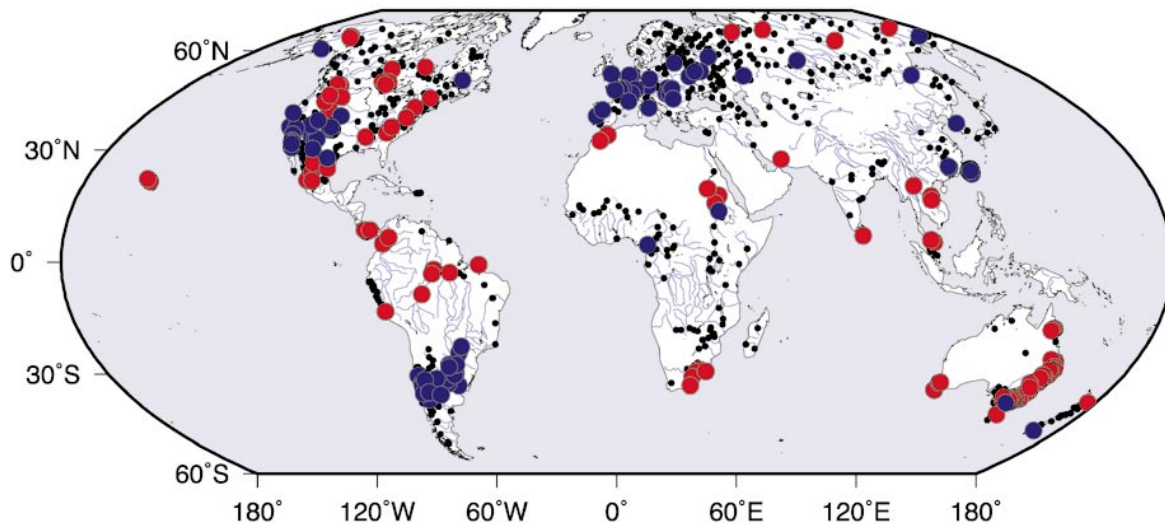
Because El Niño events and La Niña events evolve over several seasons, typically starting in boreal spring and summer and maturing in boreal winter, SOIs from preceding summers correlate almost as well with flow in the following water year in many regions as do concurrent SOIs (Fig. 12b). Some weakening of correlations at this long lead occurs in European rivers, whereas African and Southeast Asian connections are enhanced by considering the boreal summer SOIs.

b. North Pacific climate

North Pacific sea surface temperatures respond on interannual timescales to tropical variations of El Niño conditions (typically with cool central North Pacific temperatures during El Niño years; e.g., Deser and Blackmon 1995) and thus may be expected to correlate with some of the same stream flow variations as does SOI. The linkage between El Niño processes and the North Pacific is not one to one, however (e.g., Latif and Barnett 1994; Lau and Nath 1996). More than 20 years ago, Namias (1976) suggested that North Pacific sea surface temperatures might have their own influence on (at least) North American climate. More recently, a number of proposals have been made with respect to independence of decadal climate fluctuations in the region from the tropical El Niño–Southern Oscillation

a) CORRELATION BETWEEN DEC-FEB SOUTHERN OSCILLATION INDEX
and same WATER-YEAR (OCT-SEPT) STREAMFLOW

[Color: Significant at $p < 0.05$; Red = Dry El Niño; blue = Wet El Niño]



b) CORRELATION BETWEEN JUNE-AUG SOUTHERN OSCILLATION INDEX
and following WATER-YEAR (OCT-SEPT) STREAMFLOW

[Same coloring scheme as above.]

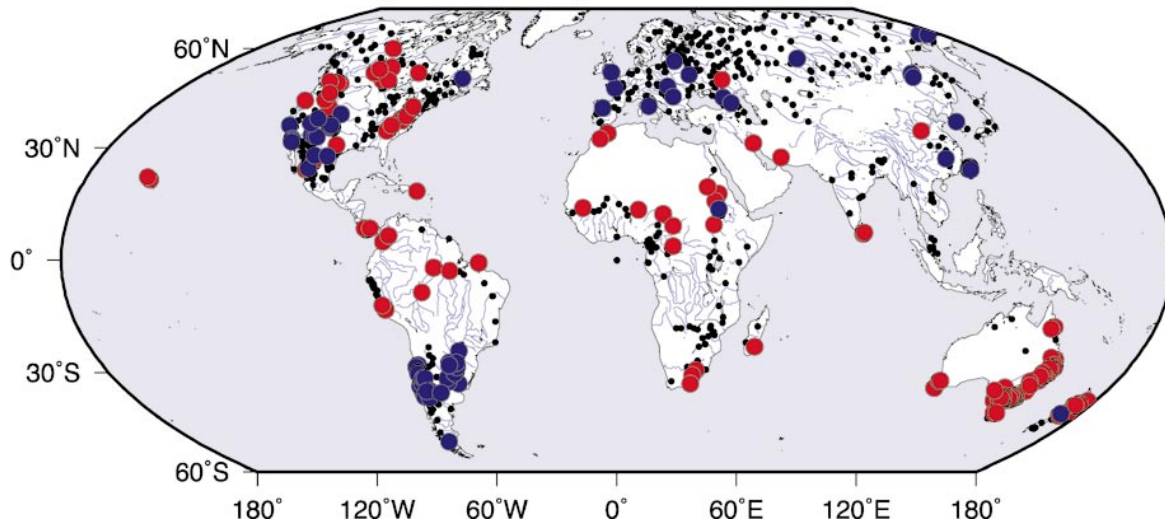


FIG. 12. Period-of-record correlations between Oct–Sep stream flows and (a) Dec–Feb Southern Oscillation index and (b) previous Jun–Aug Southern Oscillation index; colored where correlation is significantly different from zero with $p < 0.05$, red where correlation is positive (drier-than-normal El Niño years), and blue where correlation is negative (wetter-than-normal El Niño years).

processes (Jacobs et al. 1994; Latif and Barnett 1994; Gu and Philander 1997). Ting et al. (1996) and Thompson and Wallace (1998) also discussed ties between long-term fluctuations of North Pacific and North At-

lantic climates that may influence both North America and Europe.

For the periods of stream flow records available, North Pacific sea surface temperatures in the region 30°–

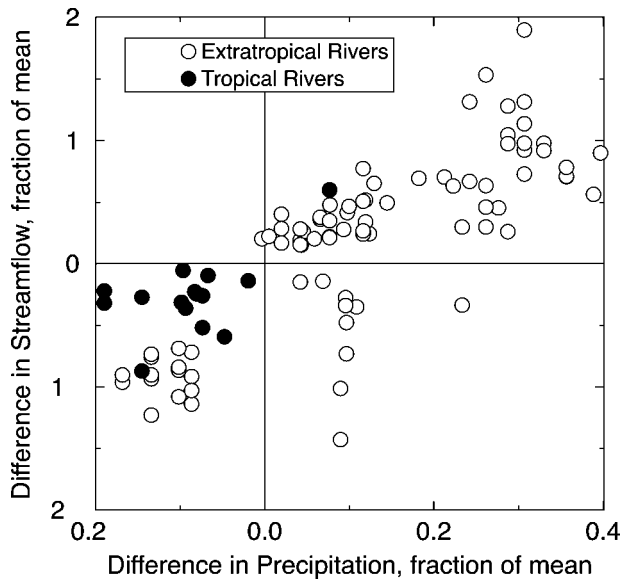


FIG. 13. Comparison of mean differences, between El Niño years and La Niña years, in stream flow and in nearest-neighbor precipitation rates in Eischeid et al. (1995) grid, as fractions of period-of-record mean annual flow and precipitation.

50°N, 150°E–120°W correlate significantly with stream flows throughout North America and Europe, as shown in Fig. 14a. Low flows dominate northern North America, Australia, and tropical South America when the central North Pacific is cool. Historically, warm central North Pacific sea surface temperatures, whether resulting from interannual or decadal climate processes, have been associated with diversions of westerly winds and low pressure systems from the midlatitude Pacific basin toward subtropical latitudes (Dettinger et al. 2000a). Indeed, the similarity between the patterns of stream flow correlation with SOI (Fig. 12a) and with the North Pacific sea surface temperatures (Fig. 14a) has been shown to result in constructive and destructive interferences of their respective teleconnection to U.S. stream flow (Gershunov et al. 1999) and in suggestions of the same interferences in river flow throughout North and South America (Dettinger et al. 2000a,b).

In addition to these influences in the Americas, rivers in Europe and tropical Africa exhibit significant correlations with the temperature of the central North Pacific. The mechanisms by which these correlations are established are uncertain, in large part because the regions also are correlated well with other climatic forcings (e.g., Africa with El Niño–Southern Oscillation; Europe with North Atlantic mechanisms) that may affect them more directly than does the North Pacific. Thus

these distant correlations may reflect shared correlations with other mechanisms rather than causal relations. Overall, though, the correlation pattern in Fig. 14 is more spatially coherent than 80%–95% of 1000 randomly distributed variants.

c. North Atlantic oscillation

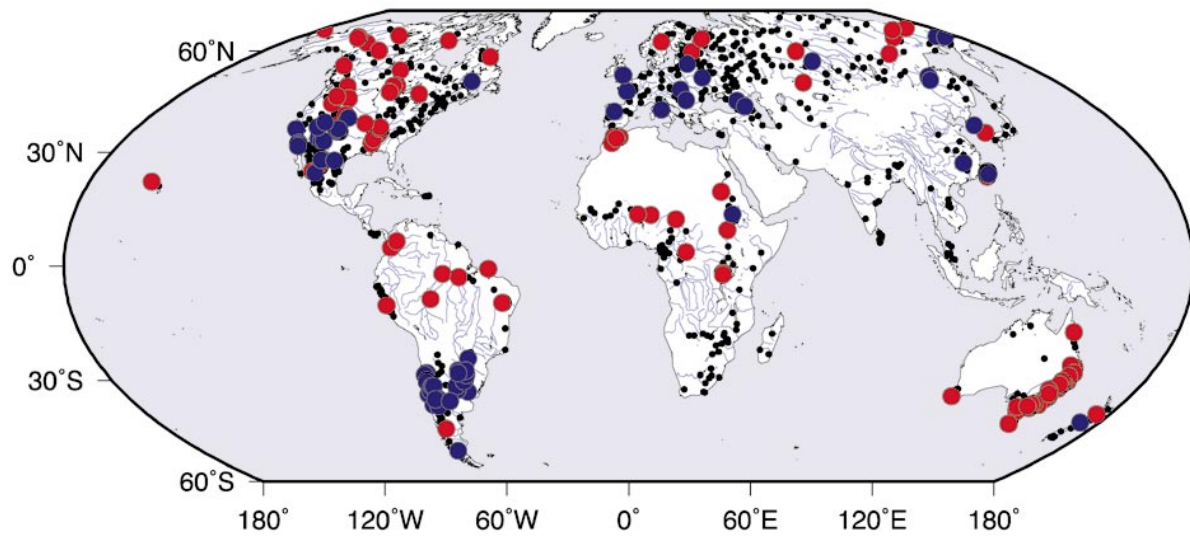
The climate of the North Atlantic region is also crucial to, at least, Northern Hemisphere climate and hydrological conditions (e.g., Hurrell 1995; Thompson and Wallace 1998). The most common measure of the North Atlantic climate is the North Atlantic oscillation index (NAO), which usually is defined as the sea level pressure difference between a site in the Azores and an Icelandic station. This pressure difference broadly reflects the strength of westerly winds across the North Atlantic between the two latitudes. When NAO is positive (anomalous pressures higher in the Azores than in Iceland), then the westerlies are strong, and winds tend to blow with greater zonality (more directly west to east) across the Atlantic. When NAO is negative, westerlies are weak with a tendency toward blocking and greater frequency of meridional winds than is normal. Under these blocked conditions, storms are steered toward northern Europe or else directly into southern Europe and North Africa. NAO is not correlated with SOI or with large-scale sea surface temperatures in the North Pacific. On decadal timescales, however, there are strong parallels between North Pacific temperatures and NAO that reflect much coherence of the Northern Hemisphere climate (e.g., Livezey and Smith 1999).

NAO is significantly correlated with stream flows in the eastern United States, Europe, and tropical Africa and America, as shown in Fig. 14b. These correlations are significantly clustered as indicated by the same spatial tests applied to, and discussed earlier in connection with, Figs. 12 and 14a. Stream flow in northernmost Europe tends to be lower than usual, and stream flow in most of the rest of Europe is higher than normal, when NAO is negative. The atmospheric state indexed by negative NAO corresponds to a southward displacement of winter storms and moisture transport across the North Atlantic into southern Europe (Hurrell 1995). A positive NAO corresponds to northward displacement of storms and moisture and thus to enhanced stream flows in northernmost Europe and Russia. In the eastern United States, winters with negative NAO are characterized by more northerly winds, which reduce moisture transports into the region from the south and, thus, reduce stream flow somewhat. Linkages between NAO and the tropical Atlantic are uncertain but probable (e.g.,

FIG. 14. (a) Period-of-record correlations between Oct–Sep stream flows and Dec–Feb sea surface temperatures in the North Pacific (averaged over 30°–50°N, 150°E–120°W); colored where correlation is significantly different from zero with $p < 0.05$, red where correlation is positive (drier than normal when North Pacific is cooler than normal), and blue where correlation is negative (wetter than normal when

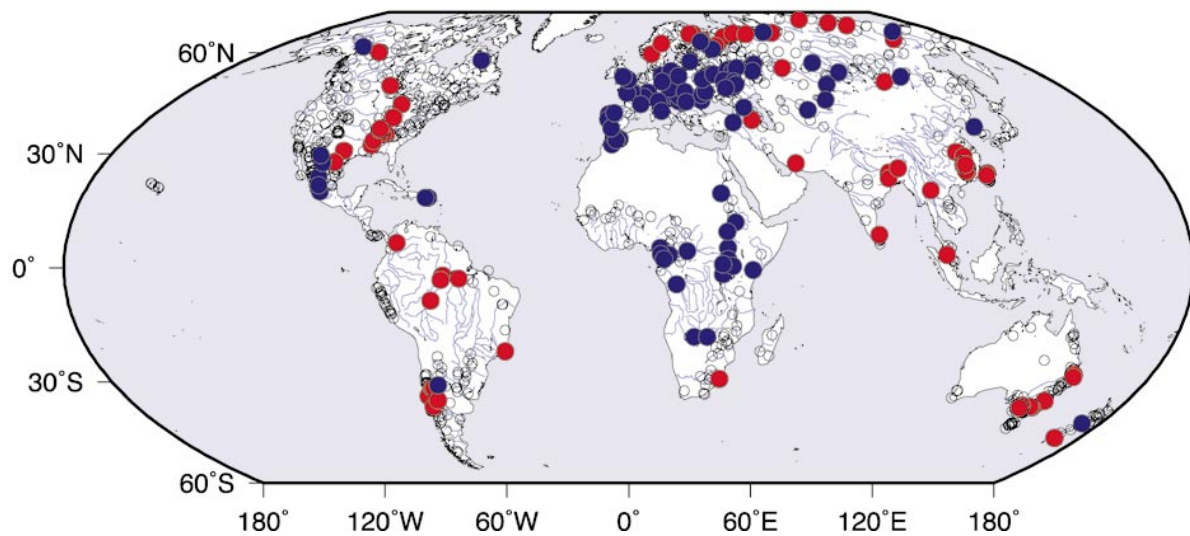
a) CORRELATION BETWEEN DEC-FEB CENTRAL NORTH PACIFIC SSTs
and WATER-YEAR (OCT-SEPT) STREAMFLOW

[Color: $p < 0.05$; Red = Dry when Pacific is cool; blue = wet]



b) CORRELATION BETWEEN DEC-FEB NORTH ATLANTIC OSCILLATION
and NORTHERN-WINTER (DEC-MAY) STREAMFLOW

[Color: $p < 0.05$; Red = Dry with negative NAO; blue = Wet]



North Pacific is cooler than normal). (b) Period-of-record correlations between Dec–May stream flows and Dec–Feb NAO index; colored where correlation is significantly different from zero with $p < 0.05$, red where correlation is positive (drier than normal when North Atlantic westerlies are weaker than normal, a negative NAO), and blue where correlation is negative (wetter than normal when North Atlantic westerlies are stronger). NAO index is the normalized difference between sea level pressures at Ponta Delgada, Azores, and Stykkisholmur, Iceland.

Wolter 1989; Hastenrath and Wolter 1992; Venske et al. 1998; Rajagopalan et al. 1998). Thus, the correlations of tropical stream flows in South America and Africa with the NAO may reflect tropical–extratropical climate connections more than they do direct ties to the North Atlantic (see Enfield and Mestas-Nuñez 1999).

Proper characterization of global-scale climate teleconnections will require much region-by-region analysis to separate the cause-and-effect connections from parallel effects, such as El Niño–Southern Oscillation effects that can masquerade as North Pacific influences. The correlation patterns shown in Figs. 12, 14a, and 14b, however, demonstrate that stream flows respond to climatic forcings on global scales, just as do regional precipitation and temperatures. Figure 13 (as well as Cayan et al. 1999) suggests that, in many settings, stream flow can respond with stronger patterns of climate teleconnections than do precipitation and temperature.

6. Summary

A dataset of monthly stream flow series from more than 1300 sites around the world (Fig. 2) has been analyzed in terms of stream flow seasonality and some aspects of interannual variability. Series were selected to provide widespread and long-term coverage that is reasonably free from human-induced discontinuities and, where possible, derived from freely distributable data sources.

Globally, at most gauges, both the timing and amplitude of stream flow seasonality depends on the local month of maximum precipitation and the extent to which precipitation is trapped in snow and ice (Figs. 3 and 5). In the eastern United States and eastern Europe, the seasonal cycle of evaporation tends to determine the stream flow timing. Lags between peak precipitation month and peak stream flow month vary relatively smoothly from long delays in high latitudes and mountainous regions to relatively short delays (0–3 months) nearly everywhere else (Fig. 4). In polar regions, the timing of runoff becomes effectively disconnected from precipitation timing and depends on the timing of summer warming; as a result, lags between precipitation and runoff peaks as great as 11 months are observed. Cluster analyses of the long-term mean monthly fractional flows in more than 1000 stream flow series identified 1) springtime ice- and snowmelt-induced streamflow maxima and 2) monsoon-induced stream flow maxima as the major contributors to overall stream flow seasonality (Fig. 3).

Mean runoff rates (stream flow per basin area; Fig. 7) and runoff efficiencies (runoff divided by gridded precipitation; Fig. 9) vary as functions of general aridity and in response to contributions from orographic sources; basin area also plays a significant role in determining runoff rates, and runoff efficiency is associated closely with runoff rate. Highest runoff rates are centered

around the tropical western Pacific, where some of the most consistent and vigorous convective precipitation falls. As would be expected, the large subtropical deserts yield the minimum runoff rates (Fig. 8). A weighted average runoff rate for the land surfaces sampled by the present dataset is 404 mm yr^{-1} . Globally, this estimate of the average runoff rate constitutes about 41% of precipitation on land areas represented by the streams and compares favorably with other estimates of continental runoff-to-precipitation rates.

Year-to-year variations in stream flow are greatest (relative to long-term mean flows) in the dry settings of the southwestern United States and Mexico, the Sahel, and the southern continents and are proportionally larger than the variations of precipitation that drive them (Fig. 10). Tropical rivers have the most (relatively) steady flows. Decadal [e.g., $<(7 \text{ yr})^{-1}$] variations in stream flow make particularly large contributions to year-to-year stream flow variance in rivers in Africa, northern Canada, and parts of South America. Interannual [e.g., $>(7 \text{ yr})^{-1}$] precipitation and stream flow variations make particularly large contributions in tropical South America and Australia, as well as in the southwestern and eastern United States, much of Europe, and northern Asia. In most regions, decadal and interannual contributions of stream flow variance are of comparable magnitude (Fig. 11).

Correlations between annual stream flow totals and climatic indices such as the Southern Oscillation index and North Atlantic oscillation illustrate global stream flow teleconnections. Seasonal SOIs are correlated to stream flows throughout the Americas, Europe, and Australia (Fig. 12). Differences in mean runoff from El Niño years to La Niña years are about five times larger (relative to mean flows) than are the corresponding differences in precipitation. Tropical stream flows, in general, are less during El Niño years than during La Niña years; the effect of El Niño years and La Niña years on extratropical flows varies from region to region, mostly in response to precipitation changes (Fig. 13). The long predictive leads provided by SOI in western North America (SOI of preceding summers predicting stream flows for the following spring; e.g., Cayan and Webb 1992) also are available for South America and Australia but may fail for other regions.

Elsewhere, North Pacific sea surface temperatures (which are themselves functions of tropical Pacific conditions) are correlated well with annual stream flows throughout much of North America as well as Europe and the Tropics (Fig. 14a). Seasonal NAO variability is reflected in stream flow variability of the eastern United States, Europe, and tropical South America and Africa (Fig. 14b).

Acknowledgments. Comments from Drs. Chris Milly, U.S. Geological Survey and Geophysical Fluid Dynamics Laboratory, Princeton; Thomas Piechota, University of California, Los Angeles; and three anonymous re-

viewers helped to focus this paper. Stream flow data in the dataset came from a number of sources, including the World Meteorological Organization stream flow archive (courtesy of Roy Jenne, National Center for Atmospheric Research); the USGS Hydroclimatic Data Network (Slack and Landwehr 1992); the National Aeronautics and Space Agency Goddard Distributed Active Archive Center; University of California, Los Angeles, Center for Studies of Hydroclimatology in the Pacific Rim; National Climatic Data Center (P. Groisman); New Zealand National Institute for Water and Atmospheric Research and Electricity Corporation of New Zealand (A. McKerchar); Instituto Nacional de Recursos Naturales in Peru; National Weather Service Nile Forecast System; Evaluacion de Recursos, S.A., in Argentina (N. Garcia, University of Santa Fe); Southern Africa Development Community in Zambia (C. B. Mwasile); and other contributors. About a dozen of the series are not in public domain and come from Eletrobrás and Eletronorte, Brazil (courtesy of J. Marengo, CPTEC-INPE). This study was funded by grants from the NOAA Office of Global Programs and by the U.S. Geological Survey Global Change Hydrology Program.

REFERENCES

- Baumgartner, A., and E. Reichel, 1975: *The World Water Balance: Mean Annual Global, Continental, and Maritime Precipitation, Evaporation, and Runoff*. Elsevier Scientific, 179 pp.
- Berbery, E. H., K. E. Mitchell, S. Benjamin, T. Smirnova, H. Ritchie, R. Hogue, and E. Radeva, 1999: Assessment of land-surface energy budgets from regional and global models. *J. Geophys. Res.*, **104**, 19 329–19 348.
- Cayan, D. R., and R. H. Webb, 1992: El Niño/Southern Oscillation and streamflow in the western United States. *El Niño—Historical and Paleoclimatic Aspects of the Southern Oscillation*, H. F. Diaz and V. Markgraf, Eds., Cambridge University Press, 29–68.
- , M. D. Dettinger, H. F. Diaz, and N. Graham, 1998: Decadal variability of precipitation over western North America. *J. Climate*, **11**, 3148–3166.
- , K. T. Redmond, and L. G. Riddle, 1999: ENSO and hydrologic extremes in the western United States. *J. Climate*, **12**, 2881–2893.
- Changnon, S. A., 1987: Detecting drought conditions in Illinois. Illinois State Water Survey Circular 164-87, 36 pp. [Available from Illinois State Water Survey Library, 2204 Griffith Dr., Champaign, IL 61820.]
- Chiew, F. H. S., T. A. McMahon, and T. Piechota, 1994: El Niño/Southern Oscillation and streamflow patterns in south-east Australia. *Trans., Instit. Eng., Australia*, **36**, 285–291.
- Depetris, P. J., and S. Kempe, 1990: The impact of the El Niño 1982 event on the Parana River, its discharge and carbon transport. *Global Planet. Change*, **3**, 239–244.
- Deser, C., and M. L. Blackmon, 1995: On the relation between tropical and North Pacific sea surface temperature variations. *J. Climate*, **8**, 1677–1680.
- Dettinger, M. D., D. R. Cayan, H. F. Diaz, and D. Meko, 1998: North-south precipitation patterns in western North America on interannual-to-decadal timescales. *J. Climate*, **11**, 3095–3111.
- , D. S. Battisti, G. J. McCabe, and R. D. Garreaud, 2000a: Interhemispheric effects of interannual and decadal ENSO-like climate variations on the Americas. *Present and Past Inter-hemispheric Climate Linkages in the Americas and their Societal Effects*, V. Markgraf, Ed., Academic Press, in press.
- , D. R. Cayan, G. J. McCabe, and J. A. Marengo, 2000b: Multiscale streamflow variability associated with El Niño/Southern Oscillation. *El Niño and the Southern Oscillation—Multiscale Variability and Global and Regional Impacts*, H. F. Diaz and V. Markgraf, Eds., Cambridge University Press, 113–147.
- Diaz, A. F., C. D. Studzinski, and C. R. Mechoso, 1998: Relationships between precipitation anomalies in Uruguay and southern Brazil and sea surface temperatures in the Pacific and Atlantic Oceans. *J. Climate*, **11**, 251–271.
- Diaz, H. F., 1996: Precipitation monitoring for climate change detection. *Meteor. Atmos. Phys.*, **60**, 179–190.
- Eischeid, J. K., H. F. Diaz, R. S. Bradley, and P. D. Jones, 1991: A comprehensive precipitation dataset for global land areas. DOE/ER-6901T-H1, TR051, 82 pp. [Available from NTIS, U.S. Dept. of Commerce, Springfield, VA 22161.]
- , C. B. Baker, T. R. Karl, and H. F. Diaz, 1995: The quality control of long-term climatological data using objective data analysis. *J. Appl. Meteor.*, **34**, 2787–2795.
- Eltahir, E. A. B., 1996: El Niño and the natural variability in the flow of the Nile River. *Water Resour. Res.*, **32**, 131–137.
- Enfield, D. B., and A. M. Mestas-Núñez, 1999: Multiscale variabilities in global sea surface temperatures and their relations with tropospheric climate patterns. *J. Climate*, **12**, 2719–2733.
- Gershunov, A., T. P. Barnett, and D. R. Cayan, 1999: North Pacific interdecadal oscillation seen as factor in ENSO-related North American climate anomalies. *Eos, Trans. Amer. Geophys. Union*, **80**, 25, 29, 30.
- Gu, D. F., and S. G. H. Philander, 1997: Interdecadal climate fluctuations that depend on exchanges between the Tropics and extratropics. *Science*, **275**, 805–807.
- Guetter, A. K., and K. P. Georgakakos, 1996: Are the El Niño and La Niña predictors of the Iowa River seasonal flow? *J. Appl. Meteor.*, **35**, 690–705.
- Hagemann, S., and L. Dumenil, 1996: Development of a parameterization of lateral discharge for the global scale. Max-Planck-Institut für Meteorologie Rep. 219, 32 pp. [Available from Max-Planck-Institut für Meteorologie, Bundesstrasse 55, D-2000, Hamburg 13, Germany.]
- Hartigan, J. A., and M. A. Wong, 1979: Algorithm AS 136—A K-means clustering algorithm. *Appl. Stat.*, **28**, 100–108.
- Hastenrath, S., 1996: *Climate Dynamics of the Tropics*. Kluwer Academic, 488 pp.
- , and K. Wolter, 1992: Large-scale patterns and long-term trends of circulation variability associated with Sahel rainfall anomalies. *J. Meteor. Soc. Japan*, **70**, 1045–1055.
- Hurrell, J. W., 1995: Decadal trends in the North Atlantic Oscillation: Regional temperatures and precipitation. *Science*, **269**, 676–679.
- Jacobs, G. A., H. E. Hurlburt, J. C. Kindle, E. J. Metzger, J. L. Mitchell, W. J. Teague, and A. J. Wallcraft, 1994: Decadal-scale trans-Pacific propagation and warming effects of an El Niño anomaly. *Nature*, **370**, 360–363.
- Janowiak, J. E., A. Gruber, C. R. Kondragunta, R. E. Livezey, and G. J. Huffman, 1998: A comparison of the NCEP–NCAR reanalysis precipitation and the GPCP rain gauge–satellite combined dataset with observational error considerations. *J. Climate*, **11**, 2960–2979.
- Kalinin, G. P., 1971: *Global Hydrology*. Israel Program for Scientific Translations, 309 pp.
- Kalnay, E., and Coauthors, 1996: The NCEP/NCAR 40-Year Reanalysis Project. *Bull. Amer. Meteor. Soc.*, **77**, 437–471.
- Kaylor, R. E., 1977: Filtering and decimation of digital time series. Inst. Phys. Sci. and Tech. Rep. BN850, 14 pp. [Available from Engineering and Physical Science Laboratory, University of Maryland at College Park, College Park, MD 20740.]
- Kiladis, G. N., and H. F. Diaz, 1989: Global climatic anomalies associated with extremes of the Southern Oscillation. *J. Climate*, **2**, 1069–1090.
- Korzun, V. I., 1978: World water balance and water resources of the earth. UNESCO Studies and Reports in Hydrology 25, 663 pp. [Available from Scripps Institution of Oceanography Library, University of California, San Diego, La Jolla, CA 92093.]

- Latif, M., and T. P. Barnett, 1994: Causes of decadal climate variability over the North Pacific and North America. *Science*, **266**, 634–637.
- Lau, N. C., and M. J. Nath, 1996: The role of the “atmospheric bridge” in linking tropical Pacific ENSO events to extratropical SST anomalies. *J. Climate*, **9**, 2036–2057.
- Legates, D. R., and J. R. Mather, 1992: An evaluation of the average annual global water balance. *Geogr. Rev.*, **82**, 253–267.
- Livezey, R. E., and T. M. Smith, 1999: Covariability of aspects of North American climate with global sea surface temperatures on interannual to interdecadal timescales. *J. Climate*, **12**, 289–302.
- Logue, J. J., 1984: Regional variations in the annual cycle of rainfall in Ireland as revealed by principal component analysis. *Int. J. Climatol.*, **4**, 597–607.
- Marengo, J. A., J. Tomsella, and C. R. Uvo, 1998: Long-term streamflow and rainfall fluctuations in tropical South America: Amazonia, east Brazil, and northwest Peru. *J. Geophys. Res.*, **103**, 1775–1783.
- Maurer, E. P., D. P. Lettenmaier, and J. O. Roads, 1999: Water balance of the Mississippi River basin from a macroscale hydrologic model and NCEP/NCAR reanalysis. *Eos, Trans. Amer. Geophys. Union*, **F80**, 409–410.
- McKerchar, A. I., C. P. Pearson, and M. E. Moss, 1996: Prediction of summer inflows to lakes in the southern Alps, New Zealand, using the spring Southern Oscillation index. *J. Hydrol.*, **184**, 175–188.
- McMahon, T. A., B. L. Finlayson, A. T. Haines, and R. Srikanthan, 1992: *Global Runoff—Continental Comparisons of Annual Flows and Peak Discharges*. Catena Verlag Paperback, 166 pp.
- Morrisey, M., and N. E. Graham, 1996: Recent trends in rain gauge precipitation measurements from the tropical Pacific: Evidence for an enhanced hydrologic cycle. *Bull. Amer. Meteor. Soc.*, **77**, 1207–1219.
- Namias, J., 1976: Negative ocean–air feedback systems over the North Pacific in the transition from warm to cold seasons. *Mon. Wea. Rev.*, **104**, 1107–1121.
- Perry, G. D., P. B. Duffy, and N. L. Miller, 1996: An extended dataset of river discharges for validation of general circulation models. *J. Geophys. Res.*, **101**, 21 339–21 350.
- Philander, S. G., 1990: *El Niño, La Niña, and the Southern Oscillation*. Academic Press, 289 pp.
- Piechota, T. C., and J. A. Dracup, 1996: Drought and regional hydrologic variation in the United States: Associations with the El Niño–Southern Oscillation. *Water Resour. Res.*, **32**, 1359–1374.
- Press, W. H., B. P. Flannery, S. A. Teukolsky, and W. T. Vetterling, 1989: *Numerical Recipes—The Art of Scientific Computing (FORTRAN)*. Cambridge University Press, 702 pp.
- Probst, J. L., and Y. Tardy, 1987: Long range streamflow and world continental runoff fluctuations since the beginning of this century. *J. Hydrol.*, **92**, 289–311.
- , and —, 1989: Global runoff fluctuations during the last 80 years in relation to world temperature change. *Amer. J. Sci.*, **289**, 267–285.
- Rajagopalan, B., Y. Kushnir, and Y. M. Tourre, 1998: Observed decadal midlatitude and tropical Atlantic climate variability. *Geophys. Res. Lett.*, **25**, 3967–3970.
- Redmond, K. T., and R. W. Koch, 1991: Surface climate and streamflow variability in the western United States and their relationship to large-scale circulation indices. *Water Resour. Res.*, **27**, 2381–2399.
- Richman, M. B., 1986: Rotation of principal components. *Int. J. Climatol.*, **6**, 293–335.
- Roads, J. O., S.-C. Chen, M. Kanamitsu, and H. Juang, 1999: Surface water characteristics in NCEP global spectral model and reanalysis. *J. Geophys. Res.*, **104**, 19 307–19 327.
- Rogers, J. C., 1988: Precipitation variability over the Caribbean and tropical Americas associated with the Southern Oscillation. *J. Climate*, **1**, 172–182.
- Ropelewski, C. F., and M. S. Halpert, 1987: Global and regional scale precipitation patterns associated with the El Niño/Southern Oscillation (ENSO). *Mon. Wea. Rev.*, **115**, 2352–2362.
- , and —, 1989: Precipitation patterns associated with the high-index phase of the Southern Oscillation. *J. Climate*, **2**, 268–284.
- , and —, 1996: Quantifying Southern Oscillation–precipitation relationships. *J. Climate*, **9**, 1043–1059.
- Slack, J. R., and J. M. Landwehr, 1992: Hydro-climatic data network (HCDN): A U.S. Geological Survey streamflow dataset for the United States for the study of climate variations, 1874–1988. U.S. Geological Survey Open-File Rep. 92-129, 193 pp. [Available from U.S. Geological Survey, Books and Open-File Reports Section, Federal Ctr., Box 25286, Denver, CO 80225.]
- Thompson, D. W. J., and J. M. Wallace, 1998: The Arctic Oscillation signature in wintertime geopotential height and temperature fields. *Geophys. Res. Lett.*, **25**, 1297–1300.
- Ting, M., M. P. Hoerling, T. Xu, and A. Kumar, 1996: Northern Hemisphere teleconnection patterns during extreme phases of the zonal-mean circulation. *J. Climate*, **9**, 2614–2633.
- van der Leeden, E., 1975: *Water Resources of the World—Selected Statistics*. Port Washington Water Information Center, 568 pp.
- Venzke, S., M. R. Allen, R. T. Sutton, and D. P. Rowell, 1998: The atmospheric response over the North Atlantic to decadal changes in sea surface temperature. Max-Planck-Institut für Meteorologie Rep. 255, 46 pp. [Available from Max-Planck-Institut für Meteorologie, Bundesstrasse 55, D-2000, Hamburg 13, Germany.]
- Wolter, K., 1989: Modes of tropical circulation, Southern Oscillation, and Sahel rainfall anomalies. *J. Climate*, **2**, 149–172.
- Yevjevich, V. M., 1963: Fluctuations of wet and dry years, Part I, Research data assembly and mathematical models. Colorado State University Hydrology Paper 1, 55 pp. [Available from Department of Earth Resources, Colorado State University, Fort Collins, CO 80523.]
- Zorn, M. R., and P. R. Waylen, 1997: Seasonal response of mean monthly streamflow to El Niño/Southern Oscillation in north central Florida. *Prof. Geogr.*, **49**, 51–62.